

A New Abnormality Detection Approach for T1-Weighted Magnetic Resonance Imaging Brain Slices Using Three Planes

Mohammed Sabbih Hamoud Al-Tamimi^{1,2,*}, Ammar Sabeeh Hmoud Al-Tamimi³, Ghazali Sulong²

¹Department of Computer Science, College of Science, University of Baghdad, Baghdad, Iraq

²UTM-IRDA Digital Media Centre (MaGIC-X), Faculty of Computing, Universiti Teknologi Malaysia, Skudai, Johor Bahru, Malaysia

³Department of Computer Engineering, College of Engineering, University of Baghdad, Baghdad, Iraq

Abstract Generally, radiologists analyse the Magnetic Resonance Imaging (MRI) by visual inspection to detect and identify the presence of tumour or abnormal tissue in brain MR images. The huge number of such MR images makes this visual interpretation process, not only laborious and expensive but often erroneous. Furthermore, the human eye and brain sensitivity to elucidate such images gets reduced with the increase of number of cases, especially when only some slices contain information of the affected area. Therefore, an automated system for the analysis and classification of MR images is mandatory. In this paper, we propose a new method for abnormality detection from T1-Weighted MRI of human head scans using three planes, including axial plane, coronal plane, and sagittal plane. Three different thresholds, which are based on texture features: mean, energy and entropy, are obtained automatically. This allowed to accurately separating the MRI slice into normal and abnormal one. However, the abnormality detection contained some normal blocks assigned wrongly as abnormal and vice versa. This problem is surmounted by applying the fine-tuning mechanism. Finally, the MRI slice abnormality detection is achieved by selecting the abnormal slices along its tumour region (Region of Interest - ROI).

Keywords Magnetic Resonance Imaging, Abnormality, Texture features, Threshold, Blocks, Fine-tuning mechanism

1. Introduction

Categorically, cancer is the most frightening affliction and brain cancer is the most intricate type to treat. Consequently, good diagnosis and selection of the most appropriate treatment is of great importance. Effective treatments of brain cancers and tumours require the high quality MR images to diagnose the severity of the disease.

Lately, MRI has emerged as a useful diagnostic tool for brain and other medical images and it's the most common test for diagnosing and confirming the presence of brain tumour [1-3]. It identifies the tumour location for recommended specialist treatment options [4]. The brain being the most important part of the Central Nervous System (CNS) its structure and function must be thoroughly studied non-invasively by doctors and researchers using MRI imaging techniques [5]. Practically, MR images include both normal and abnormal (defective) slices. Firstly, it must detect the defective or abnormal slices and separate them from the normal slices. To get the true location of the

tumour, it is necessary to achieve a precise method for abnormal slices identification by excluding the normal slices. It is customary to discuss the methods for cerebral tissues extraction associated with abnormal slices classification.

The experiments were repeated on a set of digitized medical MR images collected from three different standard/challenge dataset is used to fulfill the proposed method, the experiments were repeated with three types of dataset. These three types of dataset comprehensively evaluate the performance of the proposed methods via qualitative and quantitative measures. The first two datasets are obtained via the Internet Brain Segmentation Repository (IBSR) created by the Center for Morphometric Analysis, Massachusetts General Hospital (USA), named IBSR (10Normals_T1) devoid of brain tumour, and IBSR (536_T1) contains brain tumour. These are widely used for brain tumour detection [6-22]. The third dataset named challenge MICCAI (BRATS2012-BRATS-1) is a multimodal Brain Tumour Segmentation (BRATS) challenge that is held in conjunction with the 1st international conference on Medical Image Computing and Computer Assisted Intervention (MICCAI 2012) on October 15th, 2012 in Nice, France. This dataset provides a large number of brain tumour MRI scans in which the

* Corresponding author:

m_altamimi75@yahoo.com (Mohammed Sabbih Hamoud Al-Tamimi)

Published online at <http://journal.sapub.org/ac>

Copyright © 2016 Scientific & Academic Publishing. All Rights Reserved

tumour regions are manually delineated [23-41]. Moreover, all datasets are free of noise, slice images of each type are 8 bits/pixel greyscale in Digital Imaging and Communications in Medicine (DICOM) file format. They consist of T1-weight sequence in all the three planes (i.e. Axial, sagittal and coronal plane) and contain 4567 MRI slices from 35 patients. For the IBSR (536_T1) and challenge MICCAI (BRATS2012-BRATS-1) datasets the detection of abnormal MRI slices portion ground truth by human experts is available.

2. Related Work

Radiologists analyse the MR images by visual inspection to detect and identify the presence of tumour or abnormal tissue. The huge number of such images makes this visual interpretation process labour intensive, expensive, and often erroneous. Furthermore, the sensitivity of the human eye and brain to elucidate such images reduces with the increase of number of cases, especially when only a small number of slices contain information of the affected area. Therefore, an automated system for the analysis and classification MR images is essential.

Practically, MR images include both normal and defective slices. The likelihood of detecting a premature dementia without using rigid registration of MRI is established [42]. Based on the dissimilarity matrix, a k-Nearest Neighbors (k-NN) classifier is developed. The efficiency and performance of the classifier is tested in a leave-one-out experiment on 58 images. This method achieves an efficiency of 81%. Hybrid techniques consisting of three steps including feature extraction via Discrete Wavelet Transform (DWT), reduce the dimensions size by Principal Component Analysis (PCA) and classification of the outputs using two classifiers are proposed [43]. The Artificial Neural Network (ANN) and k-NN based classifiers are used on dataset comprised of T2-weighted having axial dimension of (256×256) pixels and image size of 70 (with 10 normal and 60 abnormal). Remarkably, the number of extracted features is reduced from 1024 to seven using PCA. Accuracy as much as 97% and 98% are achieved from DWT + PCA + ANN and DWT + PCA + k-NN, respectively.

In the past, MR brain images are classified using ANN and Support Vector Machines (SVM) method [44]. The pre-processing phase involving DWT is used as input for Neural Network (NN) and SVM. The dataset consisting of T2-weighted, axial, (256×256) pixels MRI, images size 52 with 46 for abnormal (marked by Alzheimer's disease) and 6 for normal are applied, where 4761 features are extracted. The achieved accuracy of the classifier DWT + Self-Organizing Map (SOM) is 94%, DWT + SVM with linear kernel is 96.15%, DWT + SVM with polynomial kernel is 98.00% and DWT + SVM with radial basis function based kernel is 98.00%. An automatic classification of MR images for normal or abnormal tissues

is proposed [45]. This classifier follows two steps such as feature extraction by PCA and classification by the neuro fuzzy. Using an input dataset of size 35 (with 20 as training set and 15 as testing set) the accuracy of 93.33% is achieved. Yet, an accurate differentiation between the abnormal and normal MRI slices requires dedicated research efforts. Thus, it becomes the first objective of the present study.

Despite some researcher, achieved high accuracy rate (overall 98%) but the experiments are performed with limited data sets. This paper used standard and challenge dataset to establish a strong basis and constitute a high level of reliability of the proposed net methods.

3. Methodology

This section demonstrates the new approach to separating the normal slices from the abnormal one in the brain MR images. The proposed method is comprised of four following steps: (1) Division of these tissues into non-overlapping blocks of 8×8 pixels to get a set of features for each block, (2) Determination of the optimal threshold value for splitting the blocks into normal and abnormal types, (3) Detection of abnormal block using the thresholds obtained from the step 2, and (4) Output - detected abnormal slices with its tumour region (ROI).

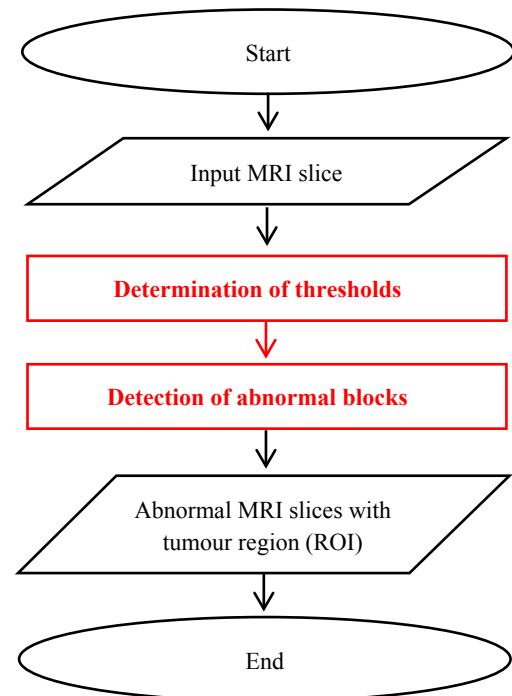


Figure 1. Flowchart of the proposed method for the detection of abnormal MRI slices

The differentiation of the abnormal MRI slices from the normal one requires the threshold value. The optimal threshold value is obtained from a statistical calculation involving three texture feature parameters such as the mean, energy, and entropy. The abnormal MRI slices can only be obtained once abnormal blocks within the slice are

successfully identified. Thus, it is prerequisite to identify the abnormal blocks and refine them in order to obtain an accurate abnormal slice. Figure 1 illustrates the flowchart of the proposed method for the detection of abnormal MRI slices.

This section contains two subsections. Subsection 3.1 describes the method for determining the optimal threshold value, followed by Subsection 3.2, which explains the detection process of tumour block abnormality in the MRI slice is emphasized.

3.1. Determination of Thresholds

The optimal threshold values are determined using statistical calculations based on the three parameters: mean, energy and entropy before the abnormality detection began. To get the optimal threshold values, finding the relationship between these features and their distribution in the MRI slice is essential. It is worth noting that all MRI slices have a similar technical specification because all of them for each patient case are obtained from the same MRI device. Furthermore, the optimal threshold value that separates healthy region from the cancerous region is calculated and determined. As mentioned earlier, each MR image consisted of a set of slices. Thus, it is necessary to choose only those slices that contain more information about cerebral tissues (Gray Matter (GM), White Matter (WM), Cerebrospinal fluid (CSF) and tumour (if any)) in the same MR image. To meet such challenges the probability calculation is carried out to select the informative slice in each MRI image, which contained all information about the cerebral tissues. Normally, the GM, WM and CSF exist in all brain slices, but the presence of the tumour is not necessary in all the slices. However, some of them reveal the presence of the tumour in the MR image, where the selection the slice having a high probability of tumour occurrence is prerequisite.

The probability distribution (frequency of occurrence) of the tumour in the slice “*i*” is obtained via the “*P*” function given by [46], [47],

$$P_i = \frac{n_i}{N} \quad (1)$$

where “*n_i*” is the number of occurrences the tumour in the slice “*i*”, and “*N*” is the total number of MR images in the dataset.

Figures 2 and 3 illustrates the probability of occurrence of the tumour in MR image slices in both IBSR (536_T1) and challenge MICCAI (BRATS2012-BRATS-1) datasets, respectively.

A visual inspection of the Figures 2 and 3 exhibits that the middle slice of each MR image achieved the highest probability equal to one (informative MRI slice). This indicates that the middle slice in each MR image contains all cerebral tissues information (GM, WM, CSF and tumour (if any)). This deductive reasoning is in line with the earlier findings [48], [49]. For that reason, this study selects only the middle MRI slices for each patient in the all datasets to determine the threshold values. This process involved three

essential steps, namely feature extraction, feature distribution, feature correlation and optimal threshold value detection.

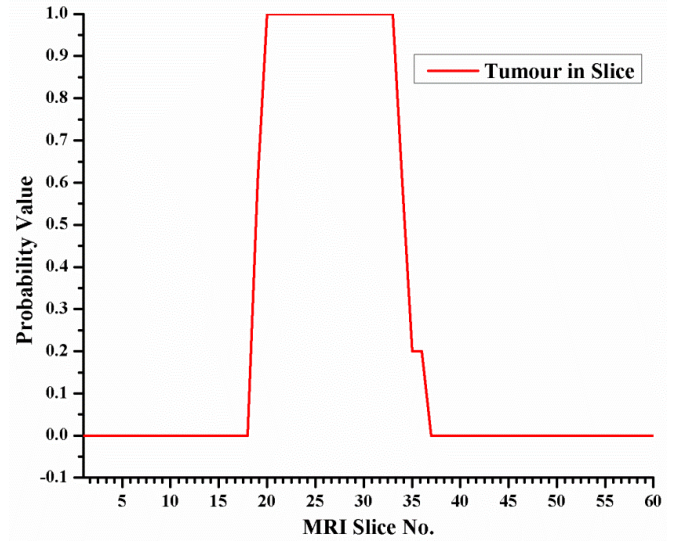


Figure 2. The probability of the tumour occurrence in MR image slices of IBSR (536_T1) dataset

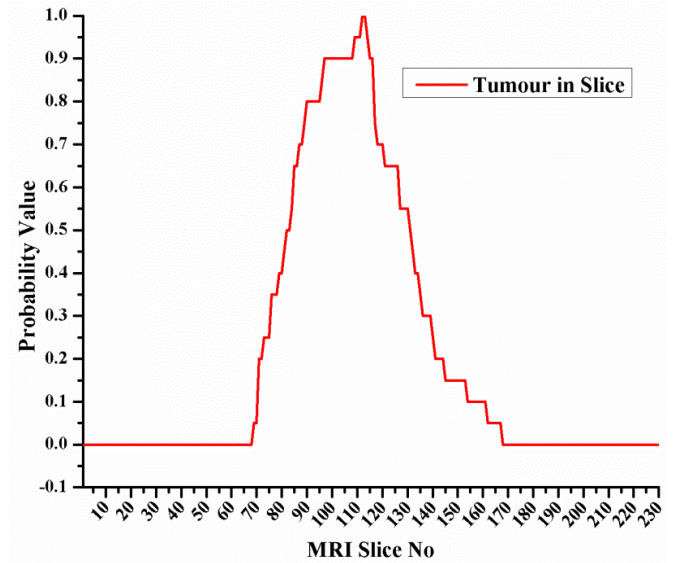


Figure 3. The probability of the tumour occurrence in MR image slices of challenge MICCAI (BRATS2012-BRATS-1) dataset

3.1.1. Features Extraction

Firstly, each of the chosen slices is partitioned into non-overlapping blocks of (8×8) pixels. This size of block is considered optimal since is empirically chosen by a set of experiments using various block sizes ranging from (4×4) to (16×16) pixels. Then, for each block, three statistical features mean, energy and entropy, are extracted to determine three threshold values, namely Mean-threshold (T1), Energy-threshold (T2), and Entropy-threshold (T3). Figures 4 and 5 depict two different examples of non-overlapping block division for MRI brain slice using (8×8) block.

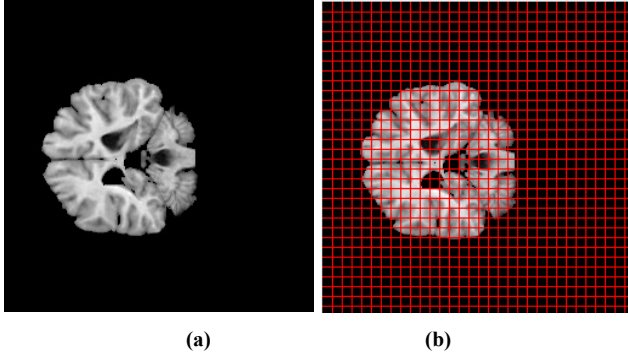


Figure 4. Non-overlapping block partition of patient Normal_19 of IBSR (10Normals_T1) dataset, (a) Original slice 23, and (b) Non-overlapping block division using (8x8) block size

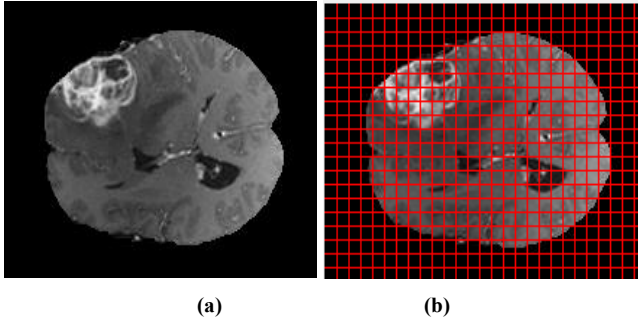


Figure 5. Non-overlapping block partition of patient BRATS_HG0009 of challenge MICCAI (BRATS2012-BRATS-1) dataset, (a) Original slice 103, and (b) Non-overlapping block division using (8x8) block size

Mean: The general brightness of an image “I” is measured using this average given by,

$$\text{Mean } (\mu) = \frac{\sum_{x=1}^w \sum_{y=1}^w I(x,y)}{w \times w} \quad (2)$$

Energy: It returns the sum of squared elements of greyscale values of all pixels in the image, which takes the value 1 for constant image and expressed as,

$$\text{Energy } (e) = \frac{1}{w \times w} \sum_{x=1}^w \sum_{y=1}^w I^2(x,y) \quad (3)$$

Entropy: It is the measure of non-uniformity in the image based on the probability of the greyscale values of all pixels and defined as,

$$\text{Entropy} = \frac{1}{w \times w} \sum_{x=1}^w \sum_{y=1}^w I(x,y) (-\ln I(x,y)) \quad (4)$$

where (w=8) is the block size.

3.1.2. Mean, Energy and Entropy Distribution

As mentioned earlier, three features such as mean, energy, and entropy are extracted from each block. A correlation between these features and their distribution in the MRI slice is determined to obtain the optimal threshold values. As previously explained (Section 3.1), the experiment is executed by taking the middle slice from each MR image, where 35 MRI slices from three data sets are selected and manually divided into non-overlapping (8x8) sub-image

blocks. Each block was labelled manually either as Normal (N) or Abnormal (A), as illustrated in Figure 6. The next step is to calculate the mean, energy, and entropy for each block using the Equations (1), (2), and (3) respectively.

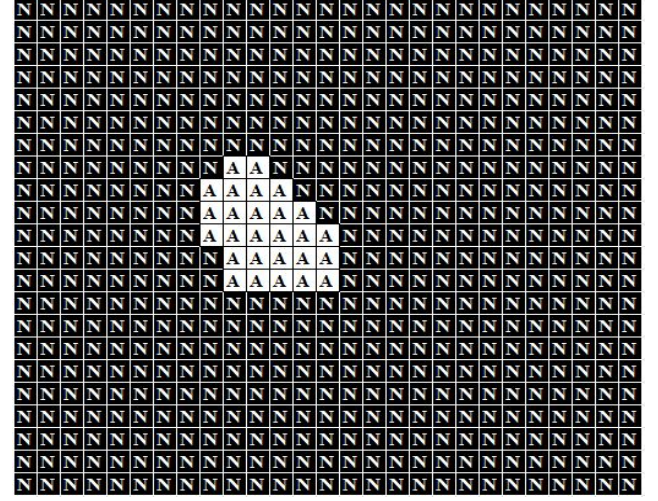


Figure 6. Manual identification of slice 88 for patient BRATS_HG0015 of challenge MICCAI (BRATS2012-BRATS-1) dataset into Normal (N) and Abnormal (A) regions

The distribution of these three features is analysed in three dimensions, where the Z axis represents the feature values, while the X and Y axes characterizes the slice image in 2D. The distribution of mean values as displayed in Figure 7 appears to be more concentrated in the abnormal region than in the normal one. This heterogeneity is attributed to the higher dispersion of white pixel distribution in the tumour region. Furthermore, the fluctuation of the mean value in the normal region is found to be widely spread within 60-120 greyscale values. Conversely, mean values in the abnormal region are stabilized between 120 and 180.

Figure 8 depicts the entropy distribution of brain slice image. They are dispersed over the entire image with relatively higher occurrence in the tumour region than the non-tumour one. The entropy value of the tumour region is discerned to be more than 500.

Figure 9 displays the energy distribution in the tumour region, which is found to be comparatively higher than the non-tumour space. Energy values of the tumour region are observed to be 14,000 times lower than the non-tumour one.

Based on the above Analysis of individual feature, we cannot ascertain the appropriate threshold value to separate tumour from non-tumour region. For that reason in-depth Analysis are required. One option is to combine the features in order to find the best combination. Various combinations are therefore performed to find the optimal threshold value. Such combinations are: (mean, energy and entropy), (mean and energy), (mean and entropy) and (entropy and energy) are used as explained in the next section.

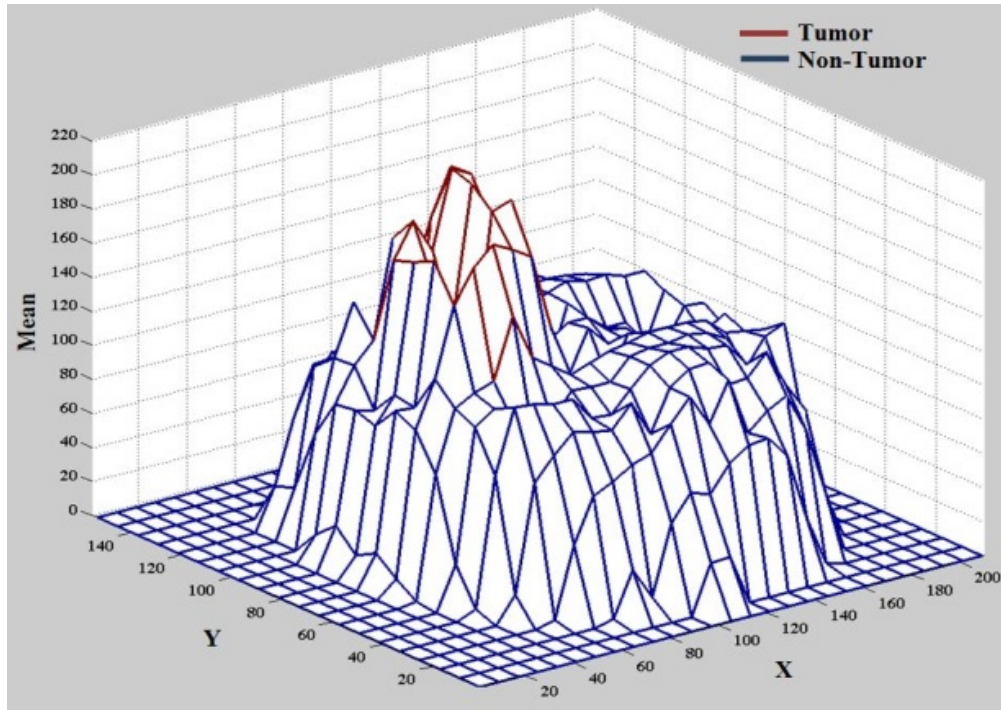


Figure 7. Distribution of mean of slice 88 for patient BRATS_HG0015 of challenge MICCAI (BRTAS2012-BRATS-1) dataset

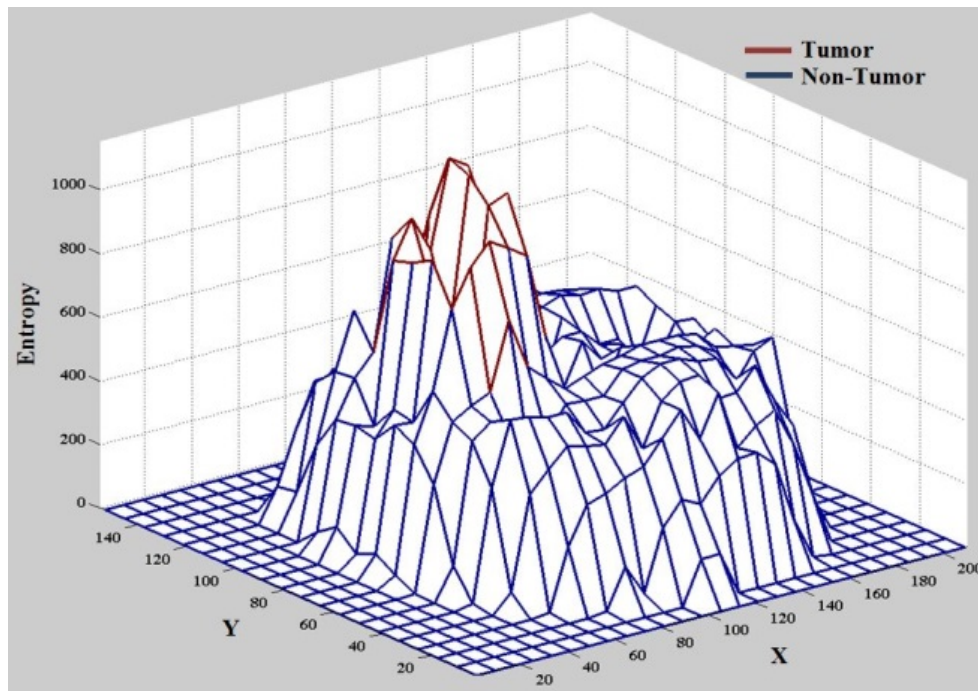


Figure 8. Distribution of entropy of slice 88 for patient BRATS_HG0015 of challenge MICCAI (BRTAS2012-BRATS-1) dataset

3.1.3. Mean, Energy and Entropy Correlation

Figure 10 shows the first combination (mean, energy and entropy). The brown stars signify the tumour region and blue one symbolizes the non-tumour zone. The figure clearly shows that when the entropy increases the tumour parts are clearly visible and well separated from non-tumour zones. This indicates that this combination of the three features performs superbly in separating the tumour from

non-tumour region – an excellent feature combination for finding the tumour.

Meanwhile, Figures 11 – 13 show the performance of the second, third and fourth combinations, respectively. Their performances resemble the first combination – almost identical.

Based on the above findings, we can deduce that: (1) The three features are significant and relevant; (2) The combinations provided identical performances in terms of

separating the tumour from non-tumour region. However, we cannot make a decision yet because the findings were only based on a single slice – is not sufficient to make a conclusion. Therefore, this study repeats the experiment for another 34 slices from all datasets to determine optimal

thresholds, T1, T2 and T3. Outcomes of the experiment are given in Table 1 below. The table reveals that T1, T2 and T3 are device-dependent because each MRI device has its own proprietary in terms of both scanner and image specifications.

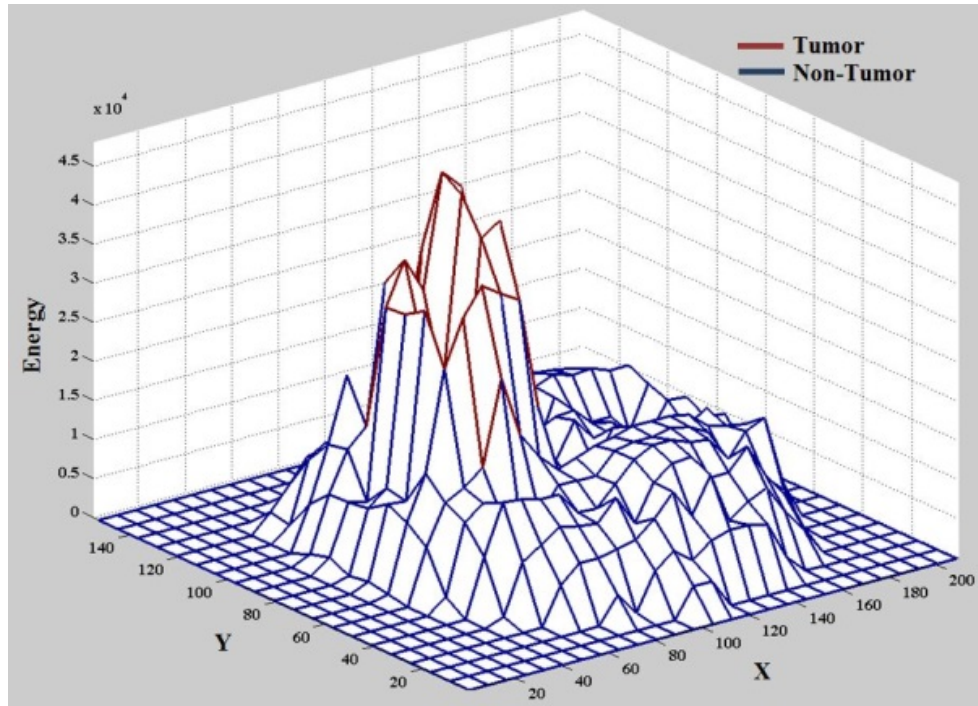


Figure 9. Distribution of energy of slice 88 for patient BRATS_HG0015 of challenge MICCAI (BRTAS2012-BRATS-1) dataset

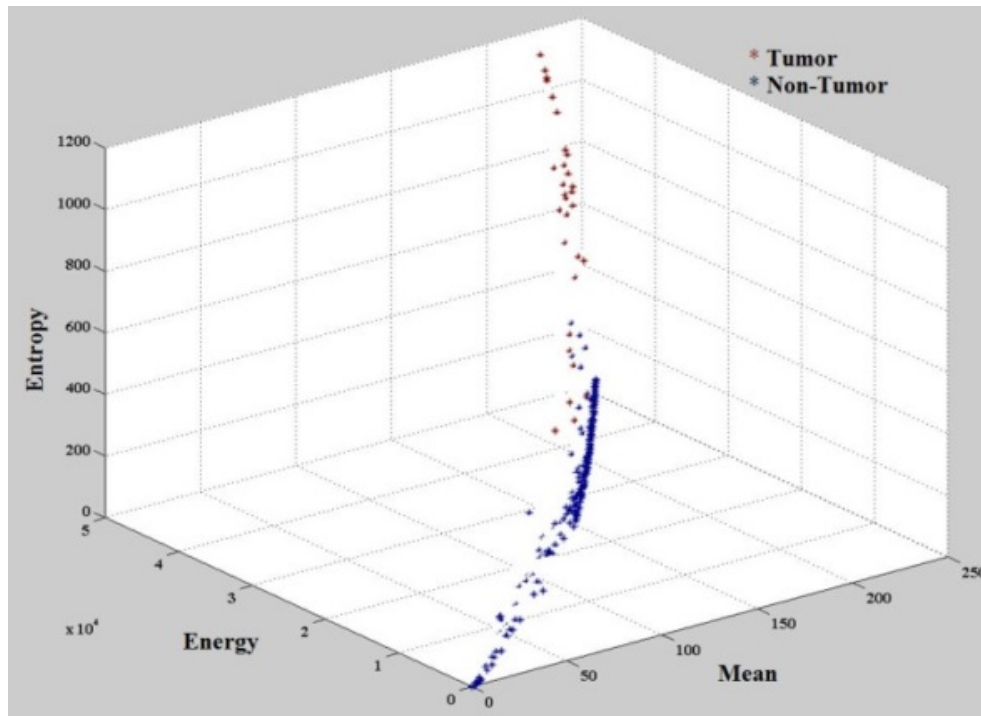


Figure 10. Relation among mean, energy, and entropy of slice 88 for patient BRATS_HG0015 of challenge MICCAI (BRTAS2012-BRATS-1) dataset

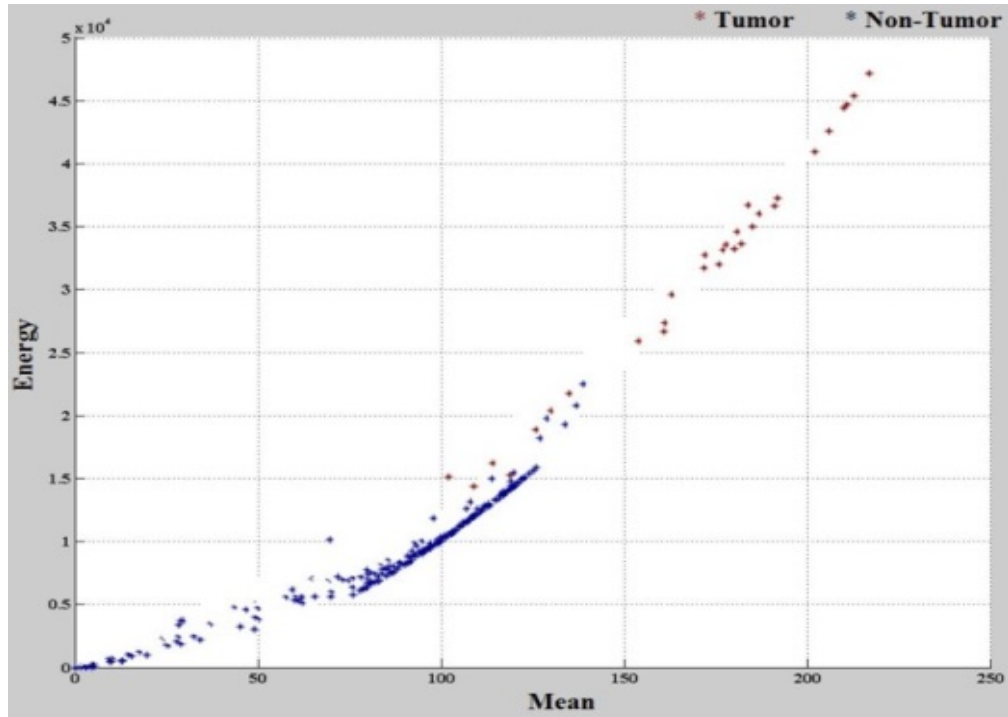


Figure 11. The relationship between mean and energy of slice 88 for patient BRATS_HG0015 in challenge MICCAI (BRTAS2012-BRATS-1) dataset

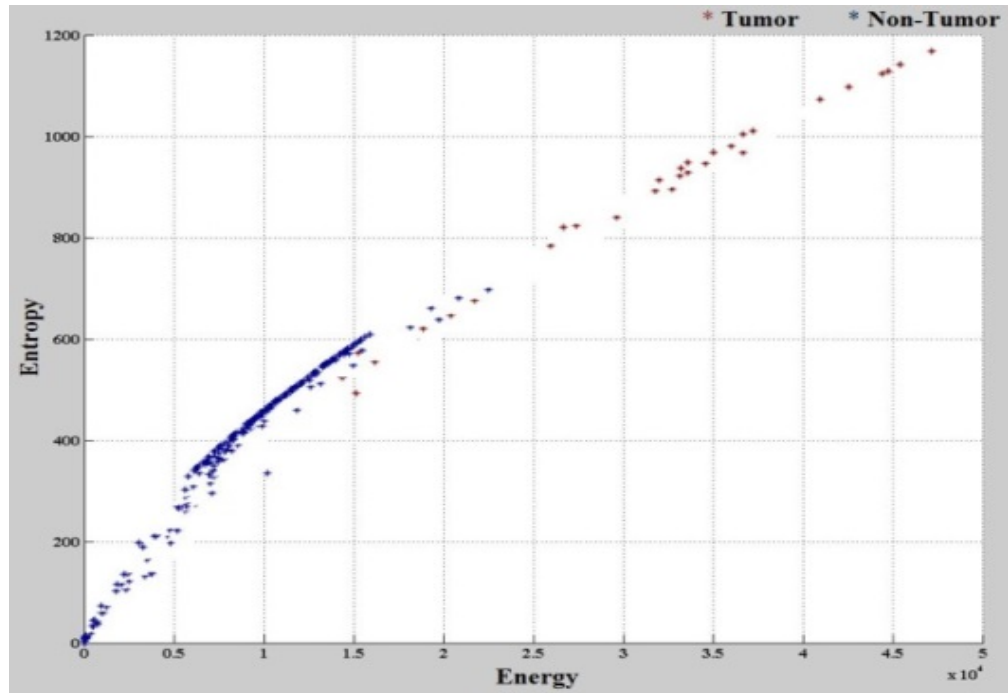


Figure 12. The relationship between entropy and energy of slice 88 for patient BRATS_HG0015 in challenge MICCAI (BRTAS2012-BRATS-1) dataset

Table 1. The threshold values of mean, energy and entropy for the different datasets

Dataset Name	Threshold Value		
	Mean (T_1)	Energy (T_2)	Entropy (T_3)
IBSR (10Normals_T1)	120	2×10^4	600
IBSR (536_T1)	120	2×10^4	600
MICCAI (BRATS2012-BRATS-1)	135	2.2×10^4	680

Note: IBSR (10Normals_T1) and IBSR (536_T1) datasets are acquired from the same MR scanner while MICCAI is from a different MR device.

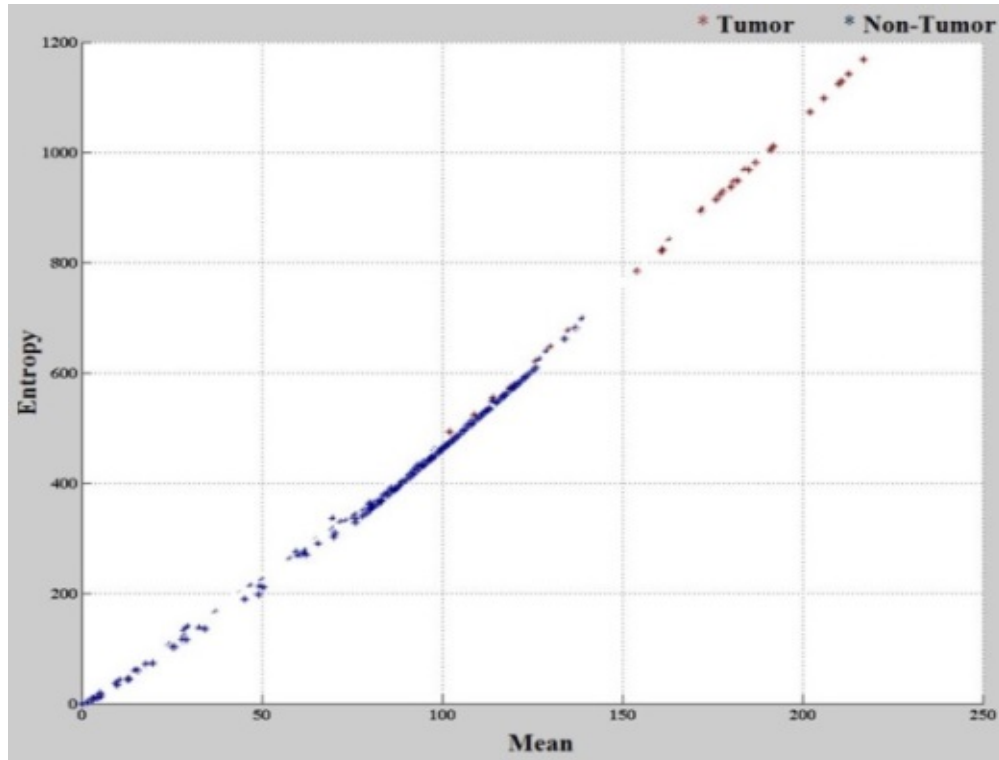


Figure 13. The relationship between entropy and mean of slice 88 for patient BRATS_HG0015 in challenge MICCAI (BRTAS2012-BRATS-1) dataset

3.2. Detection of Abnormal Blocks

Once the threshold values have been identified, the following process is to determine abnormal blocks within each MRI slice. It is obvious that if abnormal blocks are found in a particular slice, then the slice is considered as an abnormal slice. Thus, this section utilises the above thresholds, T_1 , T_2 and T_3 , to detect the abnormal blocks. A block is labelled as abnormal if and only if all the rules are satisfied. The rule is given in Figure 14.

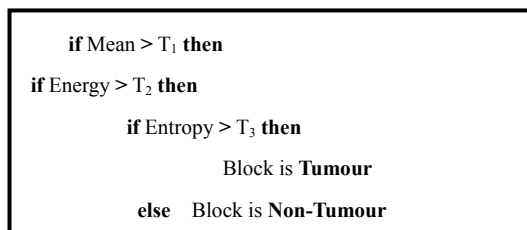


Figure 14. Abnormal block detection rules

3.2.1. Fine-tuning Mechanism of Abnormal Blocks

Undoubtedly, the above abnormality rule is simple yet efficient enough to deliver initial results. However, we cannot confirm the achieved results are 100% correct - some blocks of tumour slice images may be captured as a part of the non-tumour region, and vice versa. It is evident that the inaccuracy in the tumour block affects the results of abnormality detection of the slice. Thus, this study introduces a new technique called fine-tuning mechanism to

check, validate and improve the initial abnormal block. The fine-tuning mechanism is based on three types of (3×3) block masks, namely Preceding, Current, and Succeeding Block Mask as displayed in Figure 15.

In this procedure, the MRI slice is scanned block-by-block from the top-left to the right-bottom corners using the Current Block Mask. The mask starts from the top-left corner and moves one column at a time until it reaches the last column. Then, it moves down one row and starts again from the first column until it reaches the last column and so on so forth until it reaches the right-bottom corner.

In this study, there are fourteen scenarios, Case 1, Case 2, . . . , Case 14, may happen and need a fine-tuning. Each case is treated differently using the fine-tuning mechanism. The following paragraphs provide detailed discussions diagrammatically along with pseudo-code given in Algorithm 1 on how the mechanism works to fine-tune the problematic blocks. For ease of discussions and consistency several symbols are used, for instances, green block indicates ignored block, yellow indicates non-tumour or normal block, and red represents tumour block.

In Case 1, if a block scan reveals that all neighbouring blocks surrounding the centre block C_i are non-tumour blocks and C_i is a tumour block, then C_i become a non-tumour block to match its neighbours (see Figure 16 (a1 – a2)). Conversely, in Case 2, the mechanism changes the centre block to tumour to match its tumour neighbours (see Figure 16 (b1- b2)).

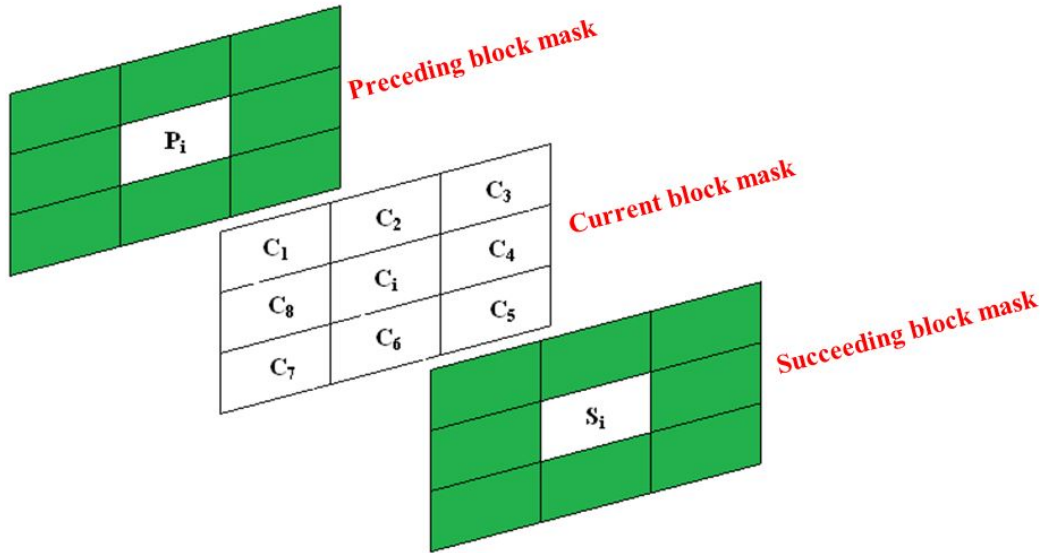
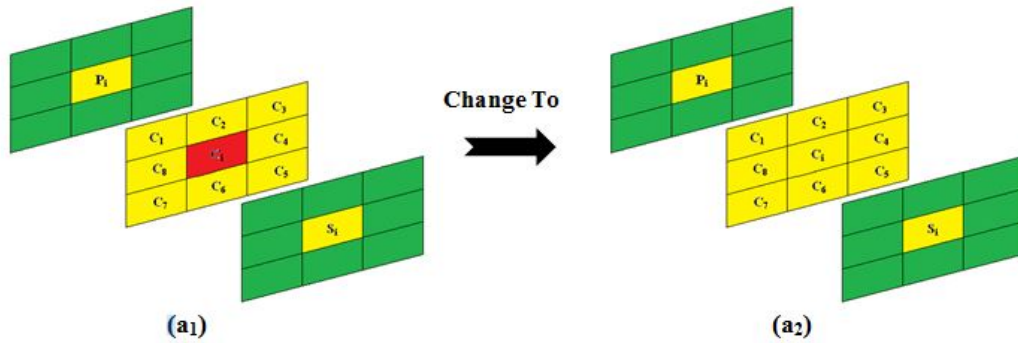


Figure 15. Three types of block masks with size (3×3) called preceding mask centred at P_i , current mask centred at C_i , and succeeding mask centred at S_i . Green colour indicates ignored block

Case 1



Case 2

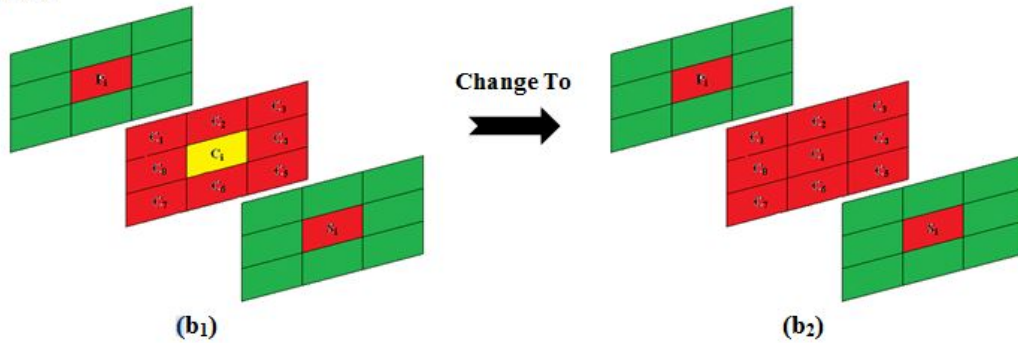


Figure 16. Fine-tuning of Case 1: (a1-a2), and Case 2: (b1-b2), where the mechanism changes the block C_i based on its neighbours

Additionally, three rules are applied to decide whether a target block C_i is the part of a tumour, or non-tumour image. Each rule is summarized as follows:

Rule 1: If centre block C_i of Current Block Mask with three of its tumour neighbours lies on one side, like Case 3: (C_1 , C_8 , C_7), Case 4: (C_1 , C_2 , C_3), Case 4: (C_3 , C_4 , C_5) or Case 6: (C_5 , C_6 , C_7) then C_i is changed to a non-tumour block (refer to Figure 17).

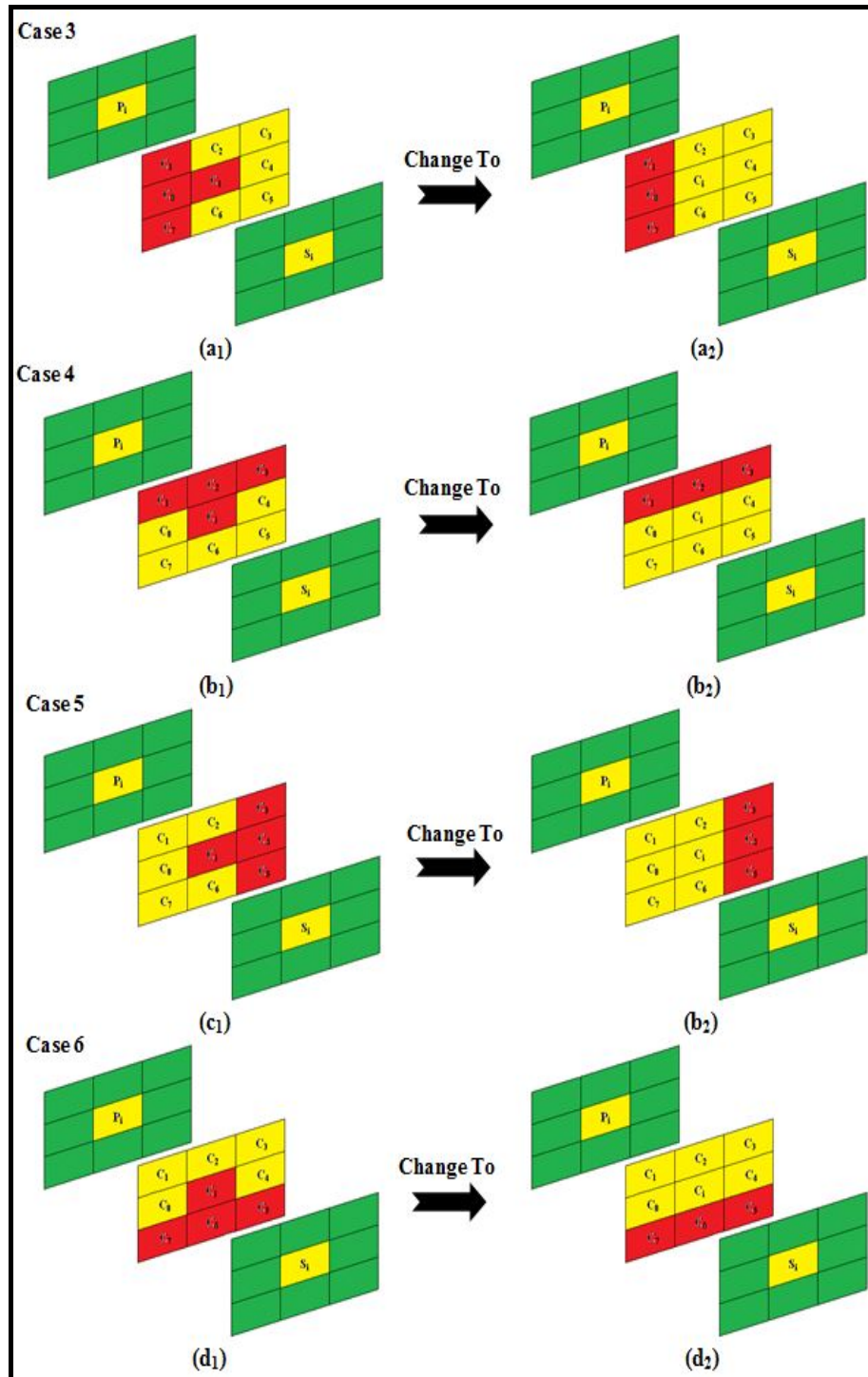


Figure 17. Fine-tuning of (Case 3 - Case 6), where C_i is changed from tumour to a non-tumour block using the Rule 1

Rule 2: If five neighbours on one side of Current Block Mask with the Preceding Block Mask and Succeeding Block Mask including Case 7: (C1, C2, C8, C7, C6, Pi, Si); Case 8: (C1, C2, C3, C4, C8, Pi, Si); Case 9: (C2, C3, C4, C5, C6, Pi, Si); or Case 10: (C4, C5, C6, C7, C8, Pi, Si) are tumour blocks and Ci is a non-tumour block, then the target block Ci becomes a tumour block as depicted in Figure 18.

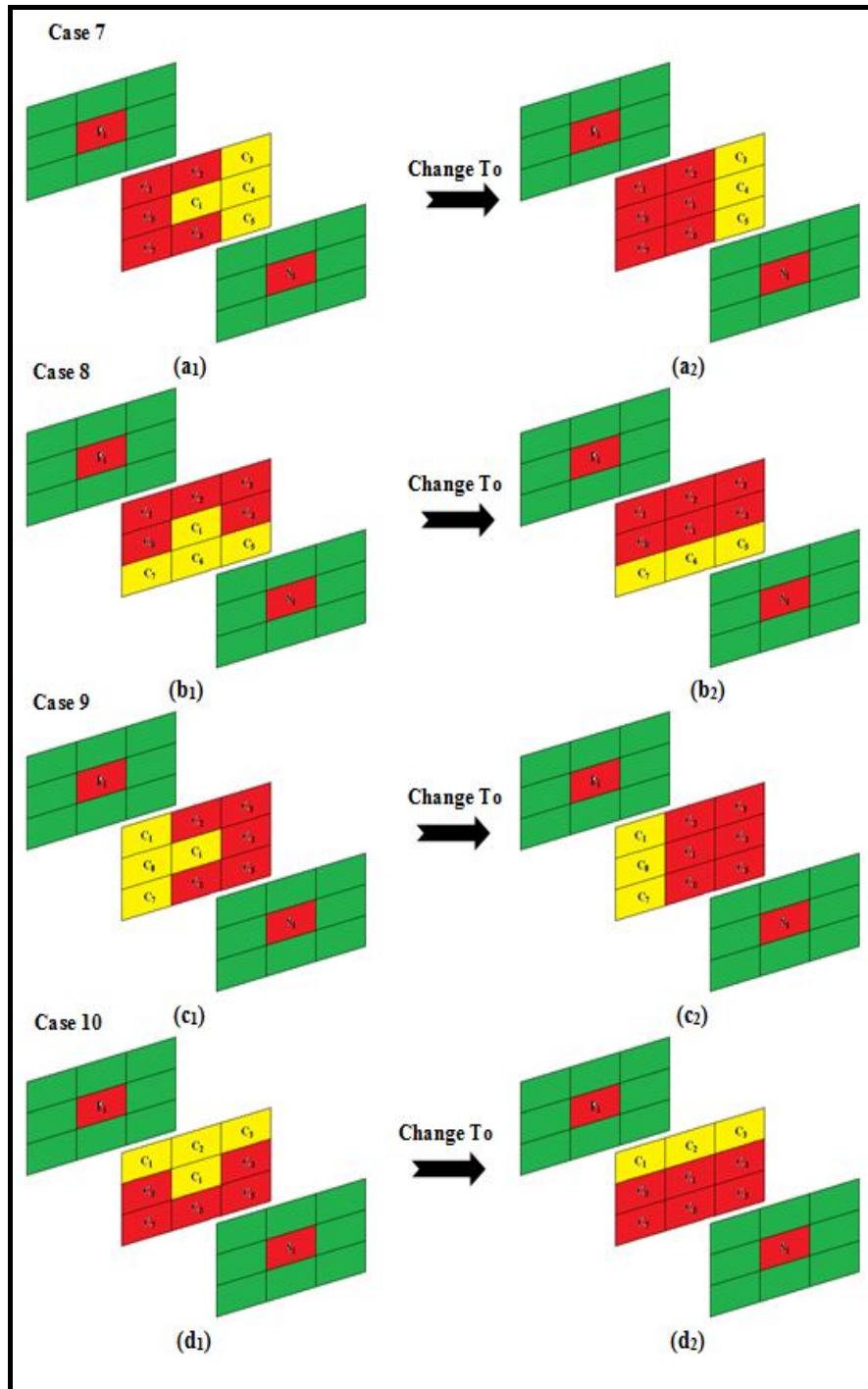


Figure 18. Fine-tuning of (Case 7 - Case 10), where C_i is changed from non-tumour to a tumour block using the Rule 2

Rule 3: If block C_i has two neighbours on opposite sides with the Preceding Block Mask and Succeeding Block Mask such as Case 11: (C_1 , C_5 , P_i , S_i); Case 12: (C_8 , C_4 , P_i , S_i); Case 13: (C_2 , C_6 , P_i , S_i); or Case 14: (C_3 , C_7 , P_i , S_i); that are tumour blocks and C_i is a non-tumour block, then the target block C_i becomes a tumour block, as shown in Figure 19.

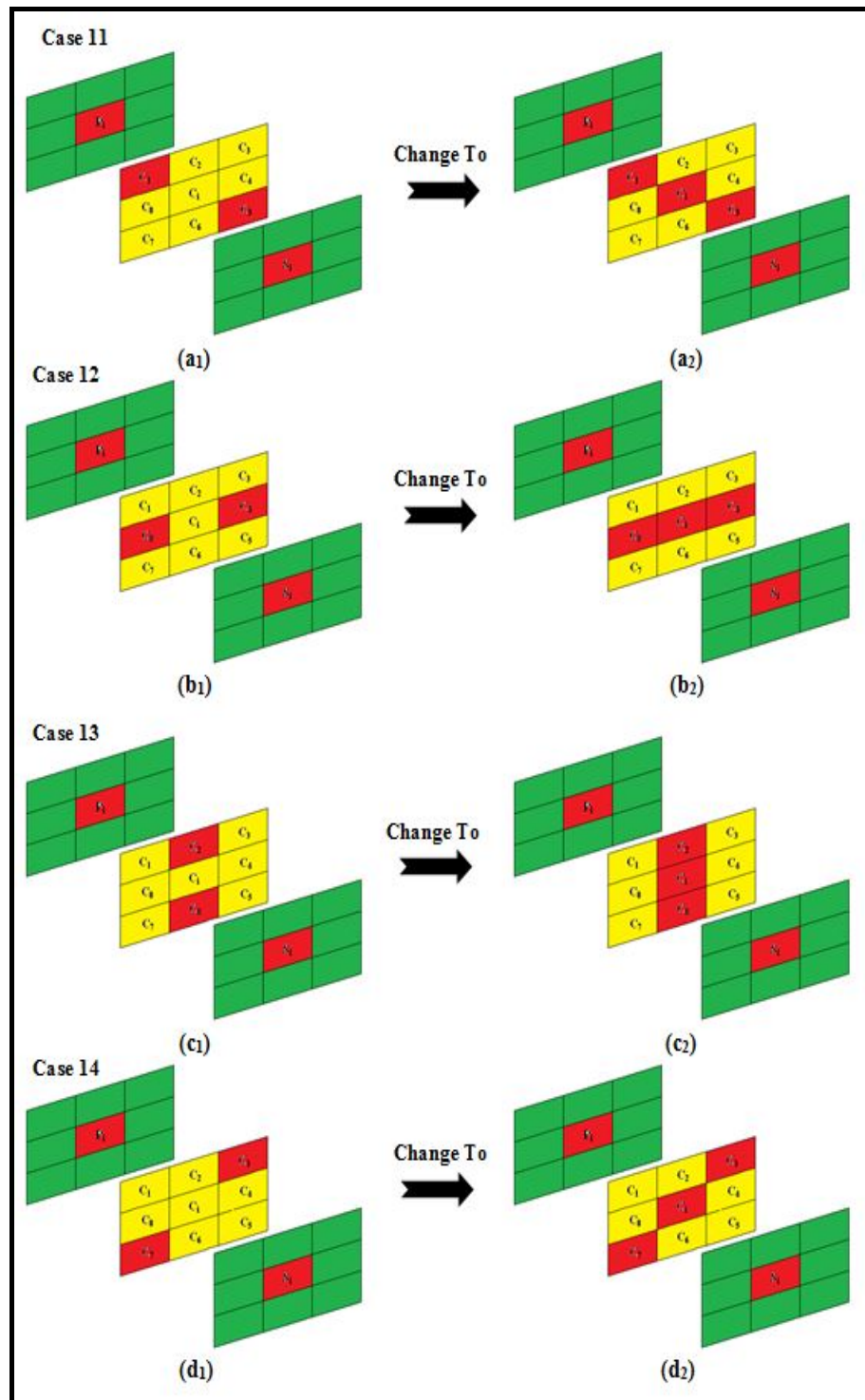


Figure 19. Fine-tuning of (Case 11 - Case 14), where C_i became a non-tumour block using the Rule 3

Once the fine-tuning of the tumour blocks completed, now it is ready to determine tumour slice based on the information gathered from the Algorithm 1. Now, once again the proposed method scans the MRI image slice by slice and calls the Fine-tuning algorithm to determine the status of the slice. The scanned slice is labelled as tumour slice if it contains at least one tumour block, otherwise the slice is considered a normal slice. The present method not only determines or detects the tumour slice, it also provides location and size (in terms of block) of tumour regions called ROI.

```

Input: N Slice Labelled Tumour Blocks (LTB) of size (H×W).
Output: N Slice improved Labelled Tumour Block(ILTB).
Variable: Preceding, Current, Succeeding, i, j, X, Y :integer.
Begin:
  for C=1 → N; increment by 1 do
    for i=1 → H; increment by 8 do
      for j=1 → W; increment by 8 do
        if all Neighbours of LTB (Current,i,j) are Non-Tumour
          if LTB (Current,i,j) is Tumour then
            ILTB (Current,i,j) ← Non-Tumour; // Case 1
          end if;
        end if;
        if all Neighbours of LTB (Current,i,j) are Tumour
          if LTB (Current,i,j) is Non-Tumour then
            ILTB (Current,i,j) ← Tumour; // Case 2
          end if;
        end if;
      end for;
    end for;
    for i=1 → H; increment by 8 do
      for j=1 → W; increment by 8 do
        if three sequence neighbours of LTB (Current,i,j) are Tumour and
          LTB (Preceding,i,j) is Non-Tumour and LTB (Succeeding,i,j) is Non-
          Tumour and the rest are all Non-Tumour then
          if LTB (Current,i,j) is Tumour then
            ILTB (Current,i,j) ← Non-Tumour; // Rule 1 (Case 3 - Case 6)
          end if;
        end if;
        if three sequence neighbours of LTB (Current,i,j) are Non-Tumour and
          LTB (Preceding,i,j) is Tumour and LTB (Succeeding,i,j) is Tumour and
          the rest are all Tumour then
          if LTB (Current,i,j) is Non-Tumour then
            ILTB (Current,i,j) ← Tumour; // Rule 2 (Case 7 - Case 10)
          end if;
        end if;
      end for;
    end for;
    for i=1 → H; increment by 8 do
      for j=1 → W; increment by 8 do
        if two Neighbours X,Y of LTB (Current,i,j) are Tumour with
          |X - Y| = 4 and LTB (Preceding,i,j) is Non-Tumour and
          LTB (Succeeding,i,j) is Non-Tumour and the rest are all Non-
          Tumour
          if LTB (Current,i,j) is Tumour then
            ILTB (Current,i,j) ← Non-Tumour; // Rule 3 (Case 11 - Case 14)
          end if;
        end if;
      end for;
    end for;
  end for;
End.

```

Algorithm 1. The fine-tuning mechanism

4. Result and Discussion

Abnormality detection of MRI slices is performed by conducting a sequence of experiments to evaluate the performance of the proposed abnormal MRI slice detection. The assessment includes: (1) Abnormal block detection (before and after the fine-tuning mechanism), and (2) The abnormal slice detection. The three above-mentioned standard datasets together with the ground truth are used for the evaluation. The performance of the proposed method is measured in both qualitative and quantitatively, and the experimental results are presented hereunder.

4.1. Results of the Abnormal Block Detection before the Fine-tuning

Three features such as mean, energy and entropy are extracted from each block. The relationship between these features and their distribution in the MRI slice are analysed using Three-Dimensional (3D) graphs. Three different thresholds are established to represent these extracted features. The rules established for the extraction of the ROI tumour region from MRI slice are based on these three thresholds (Section 3.1).

The performance of the current method is evaluated with the same visual inspection procedure where MRI slices with different contrast are examined. Figures 20, 21 and 22 shows the experimental results of the block classification using the three data sets, where the left column represents the original MRI slices image, the centre is the (8×8) block division using the proposed method and the right column is block detection result where the blue colour signifies the normal region (non-tumour area) and the other blocks implies the abnormal area (tumour area).

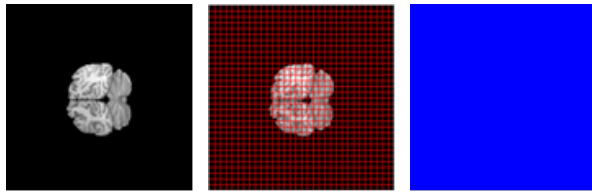


Figure 20. Abnormal block detection results of IBSR (10Normals_T1) dataset

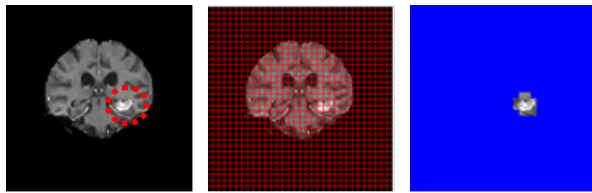


Figure 21. Abnormal block detection results of IBSR (536_T1) dataset with tumour marked by a red circle

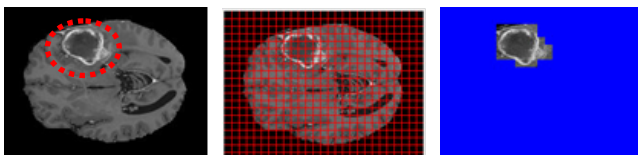


Figure 22. Abnormal block detection results challenge MICCAI (BRATS2012-BRATS-1) dataset with tumour marked by a red circle

A visual inspection of these slices clearly revealed that the proposed abnormal block detection method, in terms of the brain tumour region (a collection of tumour blocks, or in short ROI), provided reasonably excellent result. However, a few wrongly classified results, which are also termed misclassified, are obtained using the proposed method. Figures 23, 24, and 25 shows the experimental results for the three datasets, where the proposed method misclassified the block. The term misclassified is defined as "a questioned block is supposed to be tumour but the method labelled it as non-tumour, or vice versa". In this case, some blocks of tumour region are detected as non-tumour (yellow circle) and various normal blocks are appeared to be the part of the tumour region (red circle). Some misclassifications emerged with one block like the slice 13 of patient Normal_7 (Figure 23). These three cases authenticate that the current abnormal block detection process incorrectly captured the normal areas and considered them to be a part of the tumour region (red circles).

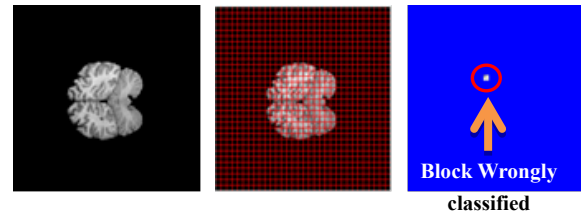


Figure 23. Misclassified blocks of IBSR (10Normals_T1) dataset without any tumour

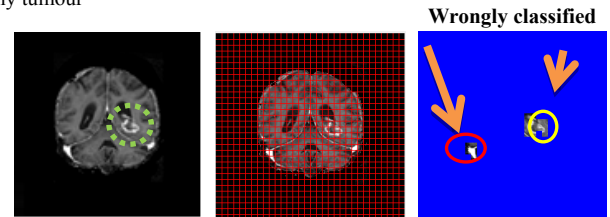


Figure 24. Misclassified blocks of IBSR (536_T1) dataset with tumour marked via green circle

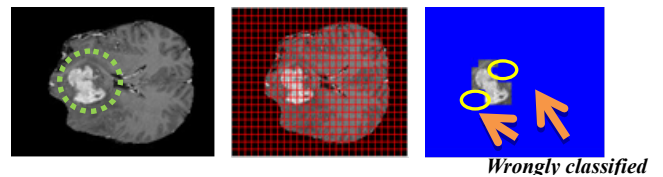


Figure 25. Misclassified blocks of challenge MICCAI (BRATS2012-BRATS-1) dataset with tumour marked via green circle

Obviously, the inaccurate identification of the tumour region greatly affects the results of slice abnormality detection. This problem is resolved by applying sets of rules based on the neighbouring blocks. First, block-by-block scanning of the MR slice image from top to bottom and from left to right direction is performed using three types of (3×3) blocks mask named "Preceding, Current, and Succeeding Blocks Mask". Next, all the neighbouring blocks surrounding a centre block in the "Current Block Mask" as well as the centred block of "Preceding, and Succeeding Blocks Mask" are selected in the final decision of the block

classification method. By applying all previously mentioned rules (Section 3.2) perfect result is achieved, where the occurrence of inexact classification blocks is corrected using the proposed method. This process is essential because the reliability of abnormality detection is primarily decided by the accuracy of this process.

Now the rules 1 and 2 based on the neighbouring blocks are applied to correct the wrong classifications. Figure 26 illustrates the corrected slices after removing the inaccuracy from patient Normal_7 (Figure 23). The first, second and third column displays the preceding slice, the current slice, and the succeeding slice, respectively.

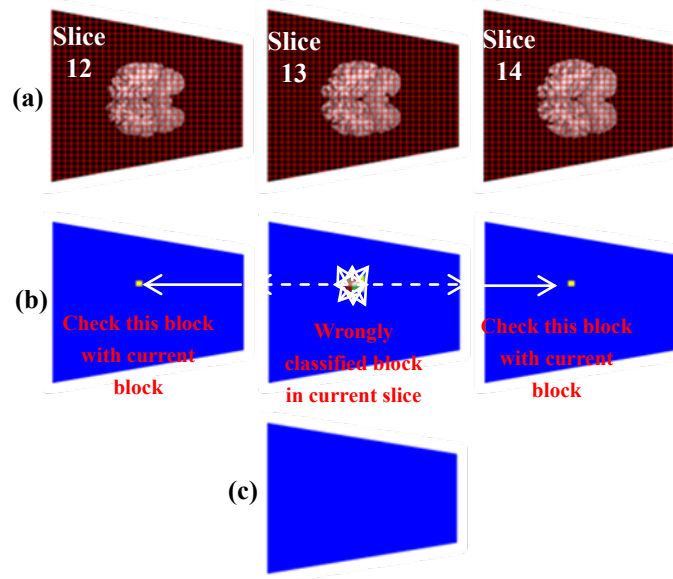


Figure 26. A fine-tuning A fine-tuning result of tumour block slice 13 of patient Normal_7 of IBSR (10Normal_T1) dataset: (a) The original non-tumour slice 13 (in grid), (b) Fine-tuning of misclassified block of the current slice, and (d) Final result of the questioned block

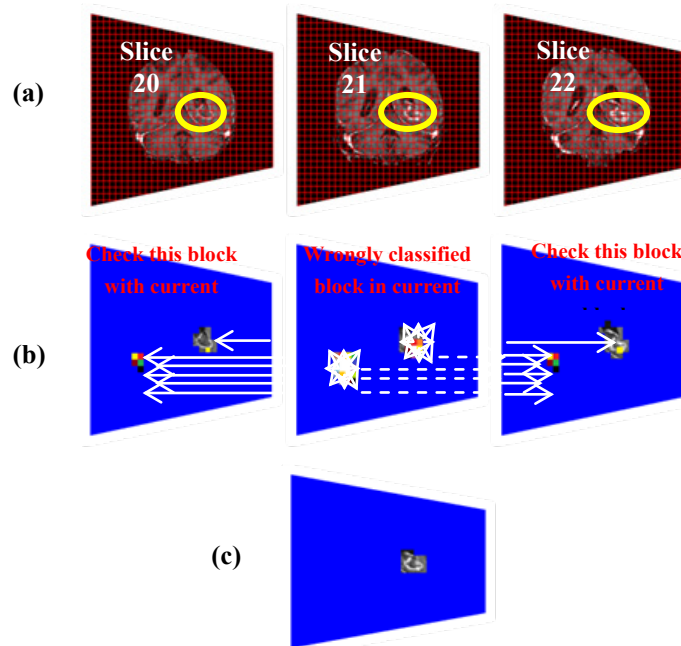


Figure 27. A fine-tuning result of six tumour blocks (two separate locations) of slice 21 of MRI scan 536_47 from IBSR (536_T1) dataset: (a) The original tumour slice 21 (in grid), (b) Fine-tuning of misclassified blocks of the current slice, and (d) Final result of the questioned blocks

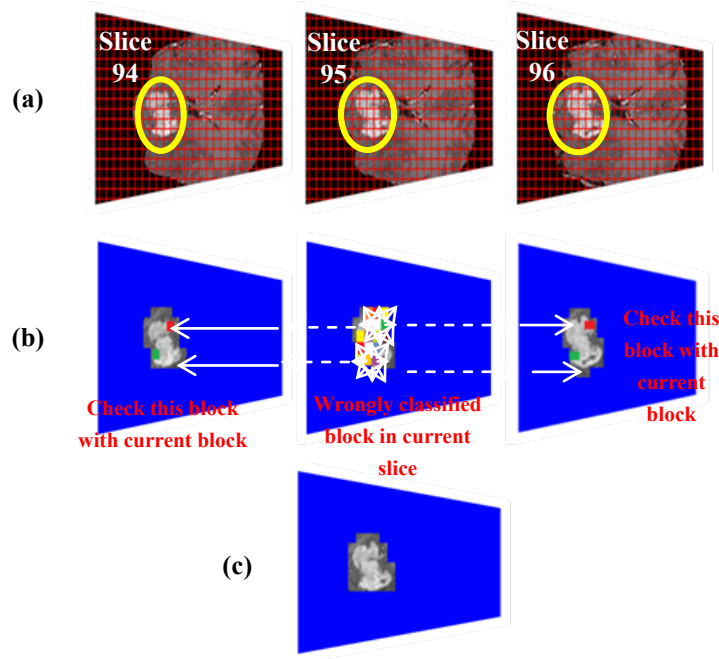


Figure 28. A fine-tuning result of two tumour blocks of slice 95 of patient BRATS_HG0015 from challenge MICCAI (BRATS2012-BRATS-1) dataset: (a) The original tumour slice 95 (in grid), (b) Fine-tuning of misclassified blocks of the current slice, and (d) Final result of the questioned block

Figure 26 clearly demonstrated that the proposed method erred in the classification of one block in each. This error is corrected based on the proposed method by using three MRI slices: the preceding slice and the succeeding slice to the current slice as shown in Figure 26(a). In the second step, it used (8×8) block division for all three slices (preceding, current and succeeding slices) as displayed in Figure 26(b). In the third step, the proposed method applied a (3×3) mask called "Current Block Mask" in the current MRI slice, where the centre of this mask is considered as the wrongly classified block. First, the test is started with all the eight surrounding blocks to determine whether these blocks are tumour blocks or not. Second, the proposed method applied another (3×3) mask called "Preceding Block Mask" on the slice (before considered as the current slice) with its centre as exactly the opposite block to block that is wrongly classified as tumour or non-tumour block. Third, a (3×3) mask named "Succeeding Block Mask" is applied on the slice that are after the current slice with its centre located exactly on the opposite block that is wrongly classified as tumour or non-tumour block as shown in Figure 26(b). Finally, it is ensured that not all the eight surrounding blocks, preceding block, and succeeding block are tumour blocks. The proposed method changed the wrongly classified block from the tumour to non-tumour one as illustrated in Figure 26(c).

It is evident that from the above findings, the proposed fine-tuning mechanism successfully solved the misclassification problems and improved the accuracy of the tumour block detection. A careful observation reveals that even complicated issues, which involved multiple blocks in two separate locations (refer to Figures 27 and 28), were solved successfully. Generally, the abnormal region contains all the important features of a tumour and any incorrectness

in the detection of this region has severe implication in terms of anomaly detection and treatment. Using the proposed abnormal block detection method coupled with the fine-tuning mechanism the tumour region is perfectly selected (i.e. ROI). Overall, in terms of the qualitative assessment, the performance of all components of the current methods, including cerebral tissue extraction, abnormality block classification and fine-tuning mechanism are satisfactory.

4.2. The Quantitative Assessment of the Tumour Block Detection

Continuing the above section, discussions are now shifted to quantitative assessment to reaffirm the above findings. For that reason, the same datasets are utilised. Two types of measures, the Jaccard (J) coefficient [50], and the Dice (D) coefficient [51] are used to validate the proposed method.

The coefficient of "J" and "D" is used to evaluate the performance of the proposed abnormal MRI slice detection method. The expression for "J" and "D" are given by:

$$J(A, B) = \frac{|A \cap B|}{|A \cup B|} \quad (6)$$

$$D(A, B) = \frac{2|A \cap B|}{|A| + |B|} \quad (7)$$

Both indices are similar. The value of "J" and "D" ranges from [0 to 1]. The performance of a method is considered perfect if both indices equalled 1 or vice versa. Both indices used two symbols, A and B. The former represents an observation result (obtained by the proposed method) while the latter symbolises a ground truth (Human expert), unless if

it stated otherwise as shown in Table 2.

Table 2. Block abnormality detection results of the IBSR (10Normals_T1)

Patient No.	No. of Block				Coefficient	
	$ A $	$ B $	$ A \cap B $	$ A \cup B $	J	D
Normal_1	54272	54272	54272	54272	1	1
Normal_4	54272	54272	54272	54272	1	1
Normal_7	54266	54272	54266	54272	0.99	0.99
Normal_8	57344	57344	57344	57344	1	1
Normal_11	54272	54272	54272	54272	1	1
Normal_15	54272	54272	54272	54272	1	1
Normal_16	57344	57344	57344	57344	1	1
Normal_17	57340	57344	57340	57344	0.99	0.99
Normal_19	57344	57344	57344	57344	1	1
Normal_20	57344	57344	57344	57344	1	1
Average					0.99	0.99

Where A: Normal block detection using the proposed method, and B: Ground truth.

In Table 2, the results have revealed that both J and D coefficients equalled 1 for over a majority of the cases. It

means that the proposed method has successfully detected non-tumour blocks in the majority of patients of this non-tumour dataset. It means that there is no tumour block found in the cases - not even a single block. However, there are exceptions for two patients named Normal_7 and Normal_17, where the proposed method misclassified six non-tumour blocks as tumour for the patient Normal_7, and four non-tumour blocks for the patient Normal_17. This is due to higher portions of whiteness ratio, which resembles a tumour block's characteristic.

Meanwhile, for the IBSR (536_T1) dataset, Figure 29 show that the achieved average coefficient for the $J \approx 0.95$ and for $D \approx 0.97$, which clearly demonstrates the superiority of the proposed method in detecting the abnormal blocks.

However, there are two wrongly classified scans, MRI scan 536_45 and MRI scan 536_47 as shown in Figures 30 and 31, respectively. In both scans, there are two misclassified blocks. However, careful observations of both figures have revealed that the cases are different: In the first case, two non-tumour blocks were classified as tumour (indicated by the red circle in Figure 30), while in the second case, two tumour blocks were misclassified as non-tumour (red circle in Figure 31).

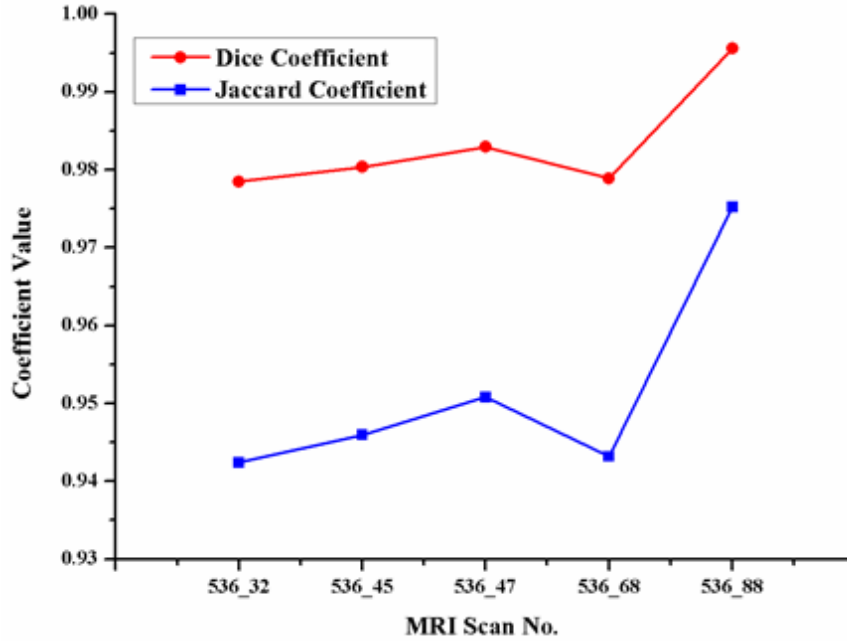


Figure 29. Block abnormality detection results of the IBSR (536_T1) dataset

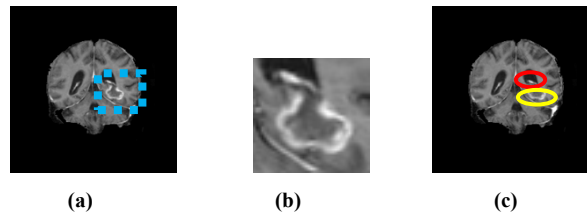


Figure 30. The misclassified MRI scan 536_45 of IBSR (536_T1) dataset, (a) Original MRI slice 22 with tumour inside the marked blue Square, (b) Zoomed in marked area, and (c) Misclassified blocks, where the red circle indicates wrongly classified blocks and yellow circle represents the tumour area

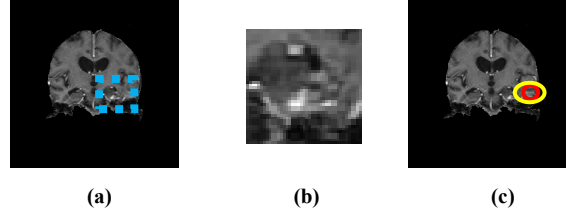


Figure 31. The misclassified MRI scan 536_47 of IBSR (536_T1) dataset, (a) Original MRI slice 31 with tumour inside marked blue Square, (b) Zoomed in marked area, and (c) Misclassified blocks, where the red circle indicates wrongly classified blocks and yellow circle represents the tumour area

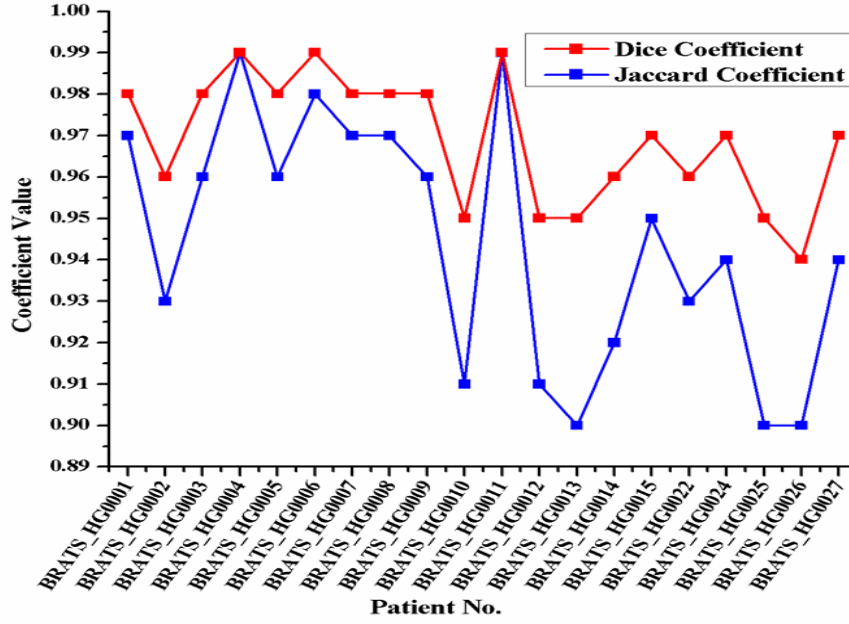


Figure 32. The Jaccard and Dice coefficients similarity indices for each MRI patient in challenge MICCAI (BRATS2012-BRATS-1) dataset

Similar excellent performance was repeated for the challenge MICCAI (BRATS2012-BRATS-1) dataset (see Figure 32), especially in terms of Dice index (average coefficient achieved is 0.97). Again, there were some misclassified blocks, particularly in patient BRATS_HG0026 where its Dice coefficient < 0.95, which affected the Dice index average.

4.3. Quantitative Evaluations of Slice Abnormality Detection

Upon completion of the assessment of the abnormal block detection, further evaluation is required to assess the performance of the proposed abnormal slice detection method. Therefore, a different set of measurements is used, namely sensitivity, specificity and accuracy to evaluate the performance of brain tumour abnormal MRI slice detection method. The formulae are as follows [52], [53]

$$\text{Sensitivity} = \frac{TP}{TP + FN} \quad (8)$$

$$\text{Specificity} = \frac{TN}{TN + FP} \quad (9)$$

$$\text{Accuracy} = \frac{TN + TP}{TN + TP + FN + FP} \quad (10)$$

Where: TP (True Positive): Number of slices that are correctly classified as abnormally slices, TN (True Negative): Number of slices that are correctly classified as normal slices, FN (False Negative): Number of normal slices those are wrongly classified as abnormally slices, and FP (False Positive): Number of abnormally slices those are wrongly classified as normal slices.

Following that, the experimental results of the proposed abnormality slice detection method, which has been implemented on the aforementioned three datasets, are given below. Again, for ease of discussion and maintaining the flow, the results and discussions are given in the same sequence as above – starting with IBSR (10Normals_T1), followed by IBSR (536_T1), and ended with challenge MICCAI (BRATS2012-BRATS-1) dataset. Also, the discussion of the results is only given in terms of sensitivity and specificity. This is in line with the medical practices [54-56].

Figure 33 has revealed perfect results for the IBSR (10Normals_T1) dataset in terms of both specificity and accuracy for almost all except two patients named: Normal_7 and Normal_17. As aforementioned, this exception is due to the misclassification of three slices for the patient Normal_7 and six slices for the patient Normal_17. These two patients contained a high whiteness ratio that resembles the tumour. The results also revealed

that the sensitivity is 0%, which indicates that there is no tumour found in all slices. This is absolutely true and 100% matched with the ground truth of the dataset.

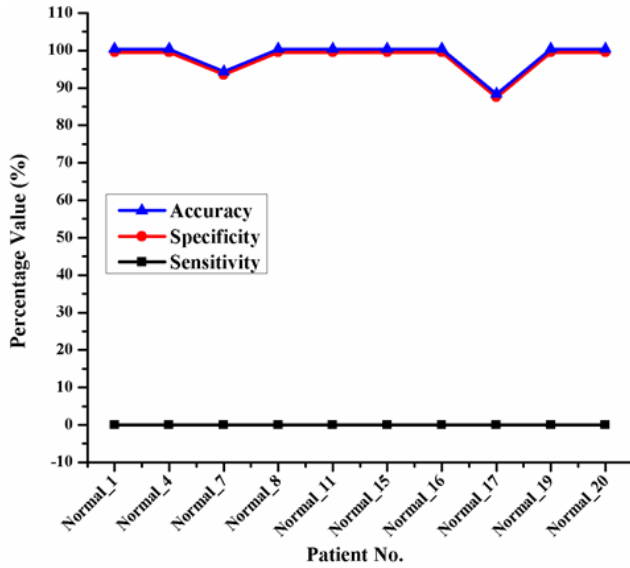


Figure 33. Experimental results of slice abnormality detection of IBSR (10Normals_T1) dataset

In the second dataset, Figure 34 has shown that almost similar performance was achieved. However, in this case, the sensitivity is 93%, which indicates that almost all slices are correctly classified as tumour slices. The remaining 7% of the slices were wrongly classified. This is due to the high intensity of healthy tissue or low intensity of cancerous tissue, where a precise demarcation could not be drawn to segregate them. Even human eyes cannot differentiate them, let alone the machine. Clinically, these such cases required further examination using another MRI sequence such as Fluid-Attenuated (FLAIR) Inversion-Recovery and intermediate-weighted sequences at MR imaging [57].

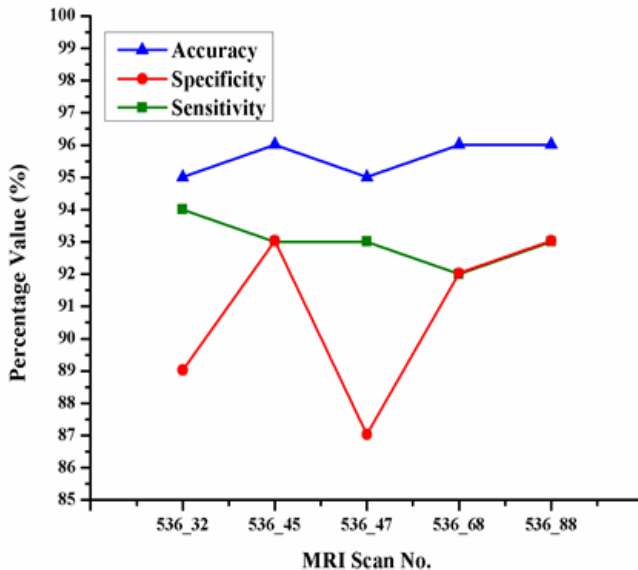


Figure 34. Experimental results of abnormality detection by slice obtained from the IBSR (536_T1) dataset

In third dataset, challenge MICCAI (BRATS2012-BRATS-1), results in Figure 35 have revealed that the sensitivity and specificity are also found to be very high. It is worth mentioning that the sensitivity is highly dependent on FN, while the specificity is dependent on FP. The misclassification in terms of FN ranged from 1.25% to 3.40%, which is considered very minimum and can be ignored - this reflects an excellent achievement. Likewise the FP (2.08% - 4.54%).

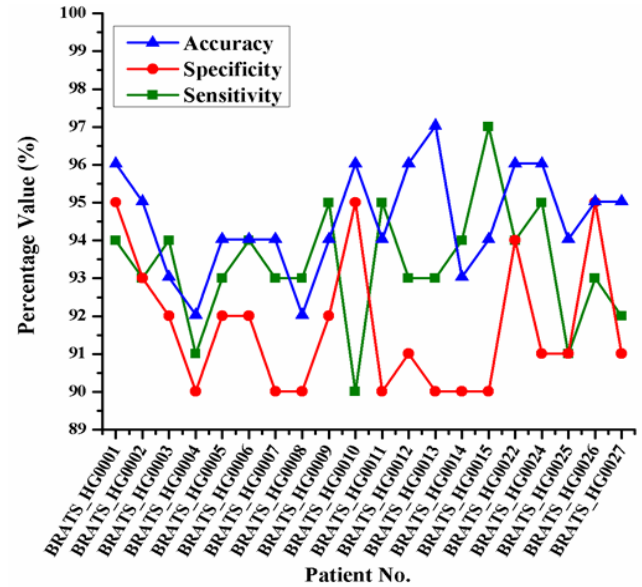


Figure 35. The sensitivity, specificity and accuracy of each MRI patient obtained from challenge MICCAI (BRATS2012-BRATS-1) dataset

Careful observation of the slices of the dataset revealed that some slices have very small tumour, which resembles low grade tumour, which is almost impossible to detect even by naked eyes.

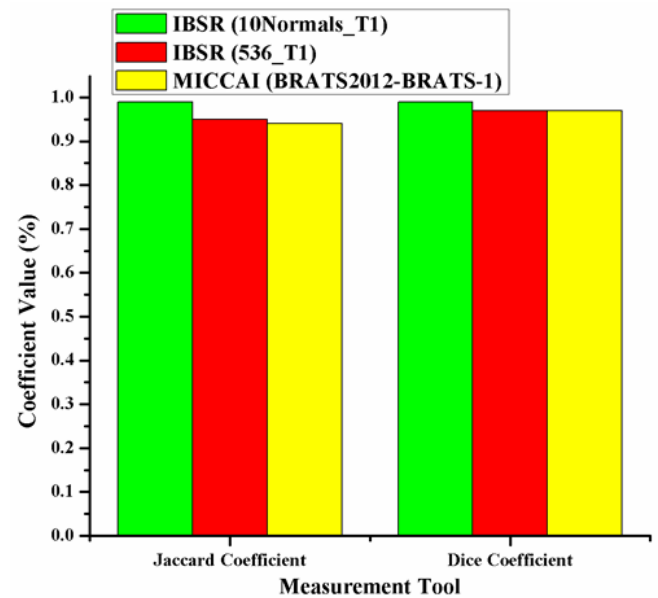


Figure 36. The measured Jaccard coefficient and Dice coefficient for the three distinct datasets: IBSR (10Normals_T1), IBSR (536_T1), and challenge MICCAI (BRATS2012-BRATS-1)

5. Conclusions

This study summarizes the above findings of the abnormal block detection, as displayed in Figure 36, to evaluate the overall performances of the proposed method. The figure reveals that the proposed method performed extremely well in all circumstances regardless of datasets.

Based on the above findings, it can be summarized that the proposed abnormal MRI slice detection method, which include abnormal block detection, has performed superbly regardless of datasets (see Figure 37).

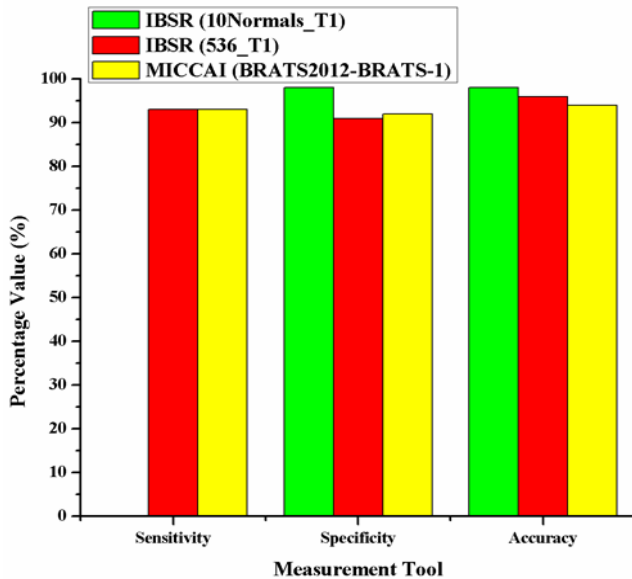


Figure 37. The Results for the sensitivity, specificity and accuracy among the three used datasets

ACKNOWLEDGEMENTS

The author(s) would like to thank the Ministry of Higher Education and Scientific Research-Iraq and University of Baghdad-Iraq for providing the financial support and facilities for this research.

REFERENCES

- [1] K. Sinha and G. R. Sinha, 2014. "Efficient Segmentation Methods for Tumor Detection in MRI Images," in *Electrical, Electronics and Computer Science (SCECS)*, 2014 IEEE Students' Conference on. IEEE, pp. 1–6.
- [2] M. S. H. Al-Tamimi and G. Sulong, 2014. "Tumor Brain Detection Through MR Images: A Review of Literature," *J. Theor. Appl. Inf. Technol.*, vol. 62, no. 2, pp. 387–403.
- [3] M. S. H. Al-Tamimi and G. Sulong, 2014. "A Review of Snake Models in Medical MR Image Segmentation," *J. Teknol.*, vol. 2, no. 1, pp. 101–106.
- [4] J. Ferlay, H. R. Shin, F. Bray, D. Forman, C. Mathers, and D. M. Parkin, 2010. "GLOBOCAN 2008, Cancer Incidence and Mortality Worldwide: IARC Cancer Base," Lyon, Fr. Int.

- Agency Res. Cancer, vol. 29, no. 10.
- [5] M. S. H. Al-Tamimi and G. Sulong, 2015. "A New Method for Detecting Cerebral Tissues Abnormality in Magnetic Resonance Images," *Mod. Appl. Sci.*, vol. 9, no. 8, pp. 363–379.
- [6] K. Sikka, N. Sinha, P. K. Singh, and A. K. Mishra, 2009. "A Fully Automated Algorithm under Modified FCM Framework for Improved Brain MR Image Segmentation," *Magn. Reson. Imaging*, vol. 27, no. 7, pp. 994–1004.
- [7] S. Bourouis and K. Hamrouni, 2010. "3D Segmentation of MRI Brain Using Level Set and Unsupervised Classification," *Int. J. Image Graph.*, vol. 10, no. 1, pp. 135–154.
- [8] J. E. Iglesias, C. Liu, P. M. Thompson, and Z. Tu, 2011. "Robust Brain Extraction Across Datasets and Comparison With Publicly Available Methods," *Med. Imaging, IEEE Trans.*, vol. 30, no. 9, pp. 1617–1634.
- [9] J. Hwang, Y. Han, and H. Park, 2011. "Skull-Stripping Method for Brain MRI Using a 3D Level Set with a Speedup Operator," *J. Magn. Reson. IMAGING*, vol. 34, no. 2, pp. 445–456.
- [10] M. A. Balafar, A. Ramli, and S. Mashohor, 2011. "Brain Magnetic Resonance Image Segmentation Using Novel Improvement for Expectation Maximizing," *Neurosciences*, vol. 16, no. 3, pp. 242–247.
- [11] F. Rousseau, P. A. Habas, and C. Studholme, 2011. "Human Brain Labeling Using Image Similarities," in *Computer Vision and Pattern Recognition (CVPR)*, 2011 IEEE Conference, pp. 1081–1088.
- [12] K. Somasundaram and T. Kalaiselvi, 2011. "Automatic Brain Extraction Methods for T1 Magnetic Resonance Images Using Region Labeling and Morphological Operations," *Comput. Biol. Med.*, vol. 41, no. 8, pp. 716–725.
- [13] O. M. Alia, R. Mandava, and M. E. Aziz, 2011. "A Hybrid Harmony Search Algorithm for MRI Brain Segmentation," *Evol. Intell.*, vol. 4, no. 1, pp. 31–49.
- [14] A. Ortiz, J. M. Górriz, J. Ramírez, and D. Salas-Gonzalez, 2011. "MR Brain Image Segmentation By Growing Hierarchical SOM and Probability Clustering," *Electron. Lett.*, vol. 47, no. 10, pp. 585–586.
- [15] G. Tian, Y. Xia, Y. Zhang, and D. Feng, 2011. "Hybrid Genetic and Variational Expectation-Maximization Algorithm for Gaussian-Mixture-Model-Based Brain MR Image Segmentation," *Inf. Technol. Biomed. IEEE Trans.*, vol. 15, no. 3, pp. 373–380.
- [16] J. Zhao, F. Q. Shao, X. D. Zhang, and C. Feng, 2012. "An Improved Integrated Active Contour Model without Re-Initialization for Vector-Valued Images Segmentation," *Adv. Mater. Res.*, vol. 429, pp. 271–276.
- [17] M. A. Balafar, 2012. "Gaussian Mixture Model Based Segmentation Methods for Brain MRI Images," *Artif. Intell. Rev.*, pp. 429–439.
- [18] L. D. Eggert, J. Sommer, A. Jansen, T. Kircher, and C. Konrad, 2012. "Accuracy and Reliability of Automated Gray Matter Segmentation Pathways on Real and Simulated Structural Magnetic Resonance Images of the Human Brain," *PLoS One*, vol. 7, no. 9, pp. 1–9.

- [19] S. Yousefi, N. Kehtarnavaz, and A. Gholipour, 2012. "Improved Labeling of Subcortical Brain Structures in Atlas-Based Segmentation of Magnetic," *Biomed. Eng. IEEE Trans.*, vol. 59, no. 7, pp. 1808–1817.
- [20] T. Zhang, Y. Xia, and D. D. Feng, 2012. "Clonal Selection Algorithm for Gaussian Mixture Model Based Segmentation of 3D Brain MR Images," *Intell. Sci. Intell. Data Eng. Springer Berlin Heidelberg*, pp. 295–302.
- [21] Z. Gang, Z. Dan, H. Ying, H. Xiaobo, Z. Yong, L. Weishi, and Z. Yang, 2013. "An Unsupervised Method for Brain MRI Segmentation," *Int. J. Emerg. Technol. Adv. Eng.*, vol. 3, no. 10, pp. 8–13.
- [22] M. S. H. Al-Tamimi, G. Sulong, and I. Lut, 2015. "Alpha Shape Theory for 3D Visualization and Volumetric Measurement of Brain Tumor Progression Using Magnetic Resonance Images," *Magn. Reson. Imaging*, vol. 33, pp. 787–803.
- [23] A. Hamamci, N. Kucuk, K. Karaman, K. Engin, and G. Unal, 2012. "Tumor-Cut: Segmentation of Brain Tumors on Contrast Enhanced MR Images for Radiosurgery Applications," *IEEE Trans. Med. Imaging*, vol. 31, no. 3, pp. 790–804.
- [24] E. D. Angelini, J. Delon, A. B. Bah, L. Capelle, and E. Mandonnet, 2012. "Differential MRI Analysis for Quantification of Low Grade Glioma Growth," *Med. Image Anal.*, vol. 16, no. 1, pp. 114–126.
- [25] Y. Megersa, 2012. "Brain Tumor Detection and Segmentation Using Hybrid Intelligent Algorithms: Design and Implementation," Addis Ababa University, Addis Ababa Institute of Technology.
- [26] Rousseau, François, P. A. Habas, and C. Studholme, 2012. "A Supervised Patch-Based Approach for Human Brain Labeling," *Med. Imaging, IEEE Trans.*, vol. 30, no. 10, pp. 1852–1862.
- [27] L. Weizman, L. Ben Sira, L. Joskowicz, S. Constantini, R. Precel, B. Shofly, and D. Ben Bashat, 2012. "Automatic Segmentation, Internal Classification, and Follow-Up of Optic Pathway Gliomas in MRI," *Med. Image Anal.*, vol. 16, no. 1, pp. 177–188.
- [28] F. C. Ghesu, M. Wels, A. Jerebko, S. Michael, J. Horneegger, and B. M. Kelm, 2014. "Integrated Spatio-Temporal Segmentation of Longitudinal Brain Tumor Imaging Studies," *Med. Comput. Vision. Large Data Med. Imaging, Springer Int. Publ.*, pp. 74–83.
- [29] L. Weizman, L. Ben Sira, L. Joskowicz, D. L. Rubin, K. W. Yeom, S. Constantini, B. Shofly, and D. Ben Bashat, 2014. "Semiautomatic Segmentation and Follow-Up of Multicomponent Low-Grade Tumors in Longitudinal Brain MRI Studies," *Med. Phys.*, vol. 41, no. 5, p. 052303.
- [30] D. Zikic, B. Glocker, E. Konukoglu, and J. Shotton, 2012. "Context-Sensitive Classification Forests for Segmentation of Brain Tumor Tissues," *Proc MICCAI-BRATS (Multimodal Brain Tumor Segmentation Challenge)*, pp. 1–9.
- [31] S. Bauer, T. Fejes, J. Slotboom, R. Wiest, L.-P. Nolte, and M. Reyes, 2012. "Segmentation of Brain Tumor Images Based on Integrated Hierarchical Classification and Regularization," *Proc MICCAI-BRATS (Multimodal Brain Tumor Segmentation Challenge)*, pp. 10–13.
- [32] E. Geremia, B. H. Menze, and N. Ayache, 2012. "Spatial Decision Forests for Glioma Segmentation in Multi-Channel MR Images," *Proc MICCAI-BRATS (Multimodal Brain Tumor Segmentation Challenge)*, pp. 14–18.
- [33] A. Hamamci and G. Unal, 2012. "Multimodal Brain Tumor Segmentation Using The 'Tumor-Cut' Method on The BraTS Dataset," *Proc MICCAI-BRATS (Multimodal Brain Tumor Segmentation Challenge)*, pp. 19–23.
- [34] L. Zhao, W. Wu, and J. J. Corso, 2012. "Brain Tumor Segmentation Based on GMM and Active Contour Method with a Model-Aware Edge Map," *Proc MICCAI-BRATS (Multimodal Brain Tumor Segmentation Challenge)*, pp. 24–27.
- [35] N. K. Subbanna and T. Arbel, 2012. "Probabilistic Gabor and Markov Random Fields Segmentation of Brain Tumours in MRI Volumes," *Proc MICCAI-BRATS (Multimodal Brain Tumor Segmentation Challenge)*, pp. 28–31.
- [36] H. Shin, 2012. "Hybrid Clustering and Logistic Regression for Multi-Modal Brain Tumor Segmentation," *Proc MICCAI-BRATS (Multimodal Brain Tumor Segmentation Challenge)*, pp. 32–35.
- [37] Y. Xiao and J. Hu, 2012. "Hierarchical Random Walker for Multimodal Brain Tumor Segmentation," *Proc MICCAI-BRATS (Multimodal Brain Tumor Segmentation Challenge)*, pp. 36–40.
- [38] X. Tomas-Fernandez and S. K. Warfiel, 2012. "Automatic Brain Tumor Segmentation Based on a Coupled Global-Local Intensity Bayesian Model," *Proc MICCAI-BRATS (Multimodal Brain Tumor Segmentation Challenge)*, pp. 41–48.
- [39] B. Menze and K. Van Leemput, 2012. "Segmenting Glioma in Multi-Modal Images using a Generative Model for Brain Lesion Segmentation," *Proc MICCAI-BRATS (Multimodal Brain Tumor Segmentation Challenge)*, pp. 49–55.
- [40] B. H. Menze, E. Geremia, N. Ayache, and G. Szekely, 2012. "Segmenting Glioma in Multi-Modal Images Using a Generative-Discriminative Model for Brain Lesion Segmentation," *Proc MICCAI-BRATS (Multimodal Brain Tumor Segmentation Challenge)*, pp. 56–63.
- [41] T. R. Raviv, K. Van Leemput, and B. H. Menze, 2012. "Multi-Modal Brain Tumor Segmentation via Latent Atlases," *Proc MICCAI-BRATS (Multimodal Brain Tumor Segmentation Challenge)*, pp. 64–73.
- [42] S. Klein, M. Loog, F. van der Lijn, T. den Heijer, A. Hammers, M. de Bruijne, A. van der Lugt, R. P. W. Duin, M. M. B. Breteler, and W. J. Niessen, 2010. "Early Diagnosis of Dementia Based On Inter subject Whole-Brain Dissimilarities," in *Biomedical Imaging: From Nano to Macro, 2010 IEEE International Symposium. IEEE.*, pp. 249–252.
- [43] E.-S. A. El-Dahshan, T. Hosny, and A.-B. M. Salem, 2010. "Hybrid Intelligent Techniques for MRI Brain Images Classification," *Digit. Signal Process.*, vol. 20, no. 2, pp. 433–441.
- [44] S. Chaplot, L. M. Patnaik, and N. R. Jagannathan, 2006. "Classification of Magnetic Resonance Brain Images Using Wavelets as Input to Support Vector Machine and Neural Network," *Biomed. Signal Process. Control*, vol. 1, no. 1, pp. 86–92.

- [45] M. Ariffanan and M. Basri, 2008. "Medical Image Classification and Symptoms Detection Using Neuro Fuzzy," PhD diss., Univ. Teknol. Malaysia, Fac. Electr. Eng.
- [46] R. Von Mises, 1964. *Mathematical Theory of Probability and Statistics*, Second Edi. Academic Press, Inc (London) LTD.
- [47] S. S. Venkatesh, 2000. *The Theory of Probability: Explorations and Applications*, First Edit. United Kingdom, Cambridge: Cambridge University Press, 2013.
- [48] V. Kuperman, *Magnetic Resonance Imaging: Physical Principles and Applications*, vol. 23, no. 2. Academic Press, Inc.
- [49] R. B. Buxton, 2009. *Introdcutin to Functional Magnetic Resonance Imaging: Principles and Techniques*, Second Edi. New York - USA: Cambridge University Press.
- [50] P. Jaccard, 1912. "The Distribution of the Flora in the Alpine Zone," *New Phytol.*, vol. XI, no. 2, pp. 37–50.
- [51] L. R.. Dice, 1945. "Measures of the Amount of Ecologic Association between Species," *Ecology*, vol. 26, no. 3, pp. 297–302.
- [52] H. Hricak, C. G. Lacey, L. G. Sandles, Y. C. Chang, M. L. Winkler, and J. L. Stern, 1988. "Invasive Cervical Carcinoma: Comparison of MR Imaging and Surgical Findings," *Radiology*, vol. 166, no. 3, pp. 623–631.
- [53] K. Hatano, Y. Sekiya, H. Araki, M. Sakai, T. Togawa, Y. Narita, Y. Akiyama, S. Kimura, and H. Ito, 1999. "Evaluation of the Therapeutic Effect of Radiotherapy on Cervical Cancer Using Magnetic Resonance Imaging," *Int. J. Radiat. Oncol. Biol. Phys.*, vol. 45, no. 3, pp. 639–644.
- [54] D. G. Altman and J. M. Bland, 1994. "Diagnostic Tests 1 Sensitivity and Specificity," *BMJ Br. Med. J.*, vol. 308, pp. 1552–1553.
- [55] G. Lalkhen and A. McCluskey, 2008. "Clinical Tests: Sensitivity and Specificity," *Contin. Educ. Anaesthesia, Crit. Care Pain*, vol. 8, no. 6, pp. 221–223.
- [56] C. J. Smith, 2012. "Diagnostic Tests (1) - Sensitivity and Specificity," *Phlebology*, vol. 27, no. 5, pp. 250–251.
- [57] and M. T. Okuda, Tomoko, Yukunori Korogi, Yoshinori Shigematsu, Takeshi Sugahara, Toshinori Hirai, Ichiro Ikushima, Luxia Liang, 1999. "Brain Lesions: When Should Recovery Sequences Be Used in MR Evaluation?," *Radiology*, vol. 212, no. 3, pp. 793–798.